NPS ARCHIVE
1998.12
HALLADAY, T.

DUDLEY KNOX LIBRARY
NAVAL POSTGRADUATE SCHOOL
MONTEREY CA 93943-5101

NAVAL POSTGRADUATE SCHOOL
Monterey, California

THESIS

MICROSTRUCTURAL CHARACTERIZATION OF TI-44AL-11NB IN THE CHILL-CAST AND DIRECTIONALLY SOLIDIFIED CONFIGURATIONS

by

Timothy R. Halladay

December 1998

Thesis Co-Advisors: Alan G. Fox
Sarath Menon

Approved for public release; distribution is unlimited.

REPORT DOCUMENTATION PAGE

Form Approved OMB No. 0704-0188

Public reporting burden for this collection of information is estimated to average 1 hour per response, including the time for reviewing instruction, searching existing data sources, gathering and maintaining the data needed, and completing and reviewing the collection of information. Send comments regarding this burden estimate or any other aspect of this collection of information, including suggestions for reducing this burden, to Washington Headquarters Services, Directorate for Information Operations and Reports, 1215 Jefferson Davis Highway, Suite 1204, Arlington, VA 22202-4302, and to the Office of Management and Budget, Paperwork Reduction Project (0704-0188) Washington DC 20503.

1. AGENCY USE ONLY *(Leave blank)*	2. **REPORT DATE** December 1998	3. **REPORT TYPE AND DATES COVERED** Master's Thesis

4. TITLE AND SUBTITLE
MICROSTRUCTURAL CHARACTERIZATION OF TI-44AL-11NB IN THE CHILL-CAST AND DIRECTIONALLY SOLIDIFIED CONFIGURATIONS

5. FUNDING NUMBERS

6. AUTHOR(S) Halladay, Timothy R.

7. PERFORMING ORGANIZATION NAME(S) AND ADDRESS(ES)
Naval Postgraduate School
Monterey CA 93943-5000

8. PERFORMING ORGANIZATION REPORT NUMBER

9. SPONSORING/MONITORING AGENCY NAME(S) AND ADDRESS(ES)
Naval Air Warfare Center, 22251 Millstone Road, Patuxent River, MD 20670

10. SPONSORING/MONITORING AGENCY REPORT NUMBER

11. SUPPLEMENTARY NOTES. The views expressed in this thesis are those of the author and do not reflect the official policy or position of the Department of Defense or the U.S. Government.

12a. DISTRIBUTION/AVAILABILITY STATEMENT
Approved for public release; distribution is unlimited.

12b. DISTRIBUTION CODE

13. ABSTRACT *(maximum 200 words)*

The microstructural evolution in chill-cast and directionally solidified Ti-44Al-11Nb (at.%) was studied by x-ray diffraction (XRD), scanning electron microscopy (SEM), and transmission electron microscopy (TEM) methods. From this data, the microstructural distribution and formation sequences of various phases like Al_3Ti, TiAl, and Ti_3Al were established. The elemental and phase distributions were determined by TEM with energy dispersive x-ray spectroscopy (EDX) and spectrum imaging. Both casting techniques produced the same phases, (Al_3Ti, TiAl, and Ti_3Al with some Nb in solid solution), but the microstructural distribution was markedly different. The chill-casting technique resulted in a coarser microstructure, with large γ crystals and duplex regions of either ($\gamma + \alpha_2$) or ($\gamma + Al_3Ti$) interspersed throughout the alloy. The directional solidification technique resulted in a much more uniform microstructure with fine lamellar grains in a dendritic macrostructure. Both casting techniques showed enrichment of niobium in interdendritic regions.

14. SUBJECT TERMS
Gamma-Titanium-Aluminum Alloys, Niobium, Intermetallics, Microstructure, Scanning Electron Microscopy, Transmission Electron Microscopy

15. NUMBER OF PAGES

16. PRICE CODE

17. SECURITY CLASSIFICATION OF REPORT	18. SECURITY CLASSIFICATION OF THIS PAGE	19. SECURITY CLASSIFICATION OF ABSTRACT	20. LIMITATION OF ABSTRACT
Unclassified	Unclassified	Unclassified	UL

NSN 7540-01-280-5500

Standard Form 298 (Rev. 2-89)
Prescribed by ANSI Std. 239-18 298-102

Approved for public release; distribution is unlimited

MICROSTRUCTURAL CHARACTERIZATION OF TI-44AL-11NB IN THE CHILL-CAST AND DIRECTIONALLY SOLIDIFIED CONFIGURATIONS

Timothy R. Halladay
Lieutenant, United States Navy
B.S.E., E.E., University of Michigan, 1987

Submitted in partial fulfillment of the
Requirements for the degree of

MASTER OF SCIENCE IN MECHANICAL ENGINEERING

from the

NAVAL POSTGRADUATE SCHOOL
December 1998

TA635
H16113
C.1
NPS ARCHIVE
1998.12
HALLADAY.T.

DUDLEY KNOX LIBRARY
NAVAL POSTGRADUATE SCHOOL
MONTEREY CA 93943-5101

ABSTRACT

The microstructural evolution in chill-cast and directionally solidified Ti-44Al-11Nb (at.%) was studied by x-ray diffraction (XRD), scanning electron microscopy (SEM), and transmission electron microscopy (TEM) methods. From this data, the microstructural distribution and formation sequences of various phases like Al_3Ti, TiAl, and Ti_3Al were established. The elemental and phase distributions were determined by TEM with energy dispersive x-ray spectroscopy (EDX) and spectrum imaging. Both casting techniques produced the same phases, (Al_3Ti, TiAl, and Ti_3Al with some Nb in solid solution), but the microstructural distribution was markedly different. The chill-casting technique resulted in a coarser microstructure, with large γ crystals and duplex regions of either ($\gamma + \alpha_2$) or ($\gamma + Al_3Ti$) interspersed throughout the alloy. The directional solidification technique resulted in a much more uniform microstructure with fine lamellar grains in a dendritic macrostructure. Both casting techniques showed enrichment of niobium in interdendritic regions.

TABLE OF CONTENTS

I. INTRODUCTION 1
II. BACKGROUND 3
A. DEVELOPMENT OF GAMMA-TITANIUM-ALUMINUM ALLOYS 3
B. POTENTIAL APPLICATIONS OF GAMMA TiAl ALLOYS 5
C. OBSTACLES TO DEVELOPMENT AND APPLICATION 7
1. Establishing Phase Diagrams 7
2. Control of Microstructure 11
3. Fracture Resistance 12
4. Creep Resistance 13
5. Fatigue Resistance 14
6. Use of Gamma TiAl at High Temperatures 15
D. EFFECTS OF ALLOYING 16
E. TITANIUM-ALUMINUM-NIOBIUM ALLOYS 19
F. DIRECTIONAL SOLIDIFICATION PROCESSING 21
III. SCOPE OF THE PRESENT WORK 25
IV. EXPERIMENTAL METHODS 27
A. METAL BUTTON INGOT FABRICATION 27
1. Chill-Cast 27
2. Directionally Solidified 27
B. SAMPLE PREPARATION 29
1. Wafer Cutting 29
2. Mechanical Grinding and Polishing 30
3. Etching 30
4. TEM Foil Preparation 31
C. X-RAY DIFFRACTION 32
D. OPTICAL MICROSCOPY 32
E. SCANNING ELECTRON MICROSCOPY (SEM) 33
F. TRANSMISSION ELECTRON MICROSCOPY (TEM) 34
V. RESULTS AND ANALYSIS 35
A. VISUAL INSPECTION AND INITIAL EVALUATION OF MATERIALS 35
1. Appearance of Coring 35
2. Homogenization of the Chill-cast Structure 36
B. ALLOY CHEMICAL COMPOSITION 39
C. X-RAY DIFFRACTION (XRD) ANALYSIS 40
D. OPTICAL MICROSCOPY 45
E. SCANNING ELECTRON MICROSCOPY (SEM) 49
F. TRANSMISSION ELECTRON MICROSCOPY (TEM) 61
VI. SUMMARY 69
A. CONCLUSIONS 69
B. RECOMMENDATIONS FOR FURTHER STUDY 70
LIST OF REFERENCES 71
INITIAL DISTRIBUTION LIST 75

ACKNOWLEDGEMENT

I would like to express my sincere gratitude and appreciation to Dr. Alan G. Fox and Dr. Sarath Menon for their tireless counsel and guidance during this thesis research.

Special acknowledgement is also due to Dr. R. Nagarajan and Mr. Rich Hashimoto for their invaluable contributions of training and laboratory assistance.

I. INTRODUCTION

Economy, efficiency of propulsion and weight reduction are vital aspects to consider in the design and construction of modern warships and aircraft in the United States Navy. Recent advances in materials technology have provided lighter, stronger structures and propulsion plants with greater power density than ever before. Engineering breakthroughs in ceramics, composites and intermetallic alloys have given design engineers a much wider range of material options to meet their needs.

Titanium-aluminum alloys have demonstrated very desirable material properties and are being investigated as potential substitutes for the more dense, conventional, nickel-based superalloys in high temperature applications, such as gas turbine engines.

The Naval Air Warfare Center (NAWC), Patuxent River, MD has combined forces with the Naval Postgraduate School in a project to investigate the development in Ti-Al-Nb alloys. These alloys are serious candidates for high temperature engine components because of their high specific strength and toughness, as well as high temperature corrosion resistance. Understanding their behavior has thus become a critical area of research for the Department of Defense. Initially, research was focused on binary gamma-TiAl alloys to determine the extent of engineering application. Unfortunately, binary gamma-TiAl alloys are far too brittle at room temperature and therefore, 11 at.% niobium has been added to gamma-TiAl to form a multi-phased ternary alloy with a complex microstructural morphology and improved ductility.

The objective of this research is to identify the phases present in a Ti-44Al-11Nb alloy in both the chill-cast and directionally solidified conditions by x-ray diffraction and to study the morphology, chemistry and interfaces in these phases using optical, scanning, and transmission electron microscopy techniques to ascertain the reason for improved ductility.

II. BACKGROUND

A. DEVELOPMENT OF GAMMA-TITANIUM-ALUMINUM ALLOYS

The first property measurements made in a binary TiAl cast alloy in the early 1950's showed the material has excellent elevated temperature properties [Ref. 1]. Since then, reports have confirmed many properties beneficial to high temperature structural applications, including low density, good high temperature strength and stiffness, thermal expansion comparable to current alloys, good oxidation resistance, and hot corrosion resistance comparable to, or better than, those of current alloys. [Ref. 2]

The first major gamma alloy development program was initiated by the Air Force Materials Laboratory and conducted by Pratt and Whitney from 1975-1983 [Ref. 3]. This exploratory program evaluated numerous compositions through wrought processing and recommended Ti-48Al-1V-(0.1C) as the best first-generation alloy composition on the basis of ductility and creep resistance. Nevertheless, the mechanical properties of the first generation gamma alloy in the fine duplex microstructure condition were not adequate for the requirements of any engine components at that time. Alloy castings were also evaluated; however, the properties were found to be unsatisfactory as the large-grained cast lamellar microstructures resulted in poor ductility and low strength. [Ref. 2]

The second major development program initiated again by the Air Force was performed by General Electric from 1986-1991. Largely based on the knowledge accumulated during the first program effort and other independent investigations, the

effort identified Ti-48Al-2(Cr or Mn)-2Nb as the best second-generation alloy composition [Ref. 4]. The alloys, produced through the rapid-solidification/wrought processing, had a fine duplex microstructure, and exhibited ductility, strength and oxidation resistance improved over those of the first-generation gamma alloy [Ref. 5]. Again, however, the alloys showed poor tensile properties for fully lamellar microstructures, which are generally large, grained [Refs. 6,7]. Understanding the effects of alloying elements, as well as, composition on the properties progressed during this period for both binary compositions and multicomponent alloy systems. [Ref. 2]

As in most metallic materials, investment casting was used as the first process route for producing experimental gamma components. For the last few years, the gamma casting technology has advanced considerably through solving various problems such as cracking, hot tearing, surface connected porosity, filling and dimensional accuracy. Much effort now appears to be directed toward establishing low cost, consistent manufacturing processes which incorporate alloy composition and its variations, materials properties, casting conditions and parameters, fillability, hot isostatic pressing (HIP), and final microstructures of interest. [Ref. 2]

In general, gamma alloys in an as-cast condition exhibit unacceptably low ductility and strength for many applications [Ref. 8], due mainly to the coarse and nonuniform cast lamellar microstructure, which is not readily removed by hot isostatic pressing. Efforts have been made to control the lamellar structure, through heat treatments, forming finer mixtures of gamma grains and residual lamellar regions, which are called 'casting duplex' microstructures [Ref. 8], and possess a reasonable balance of properties. [Ref. 2]

Data bases for the second-generation cast alloys are being established through extensive property evaluation on a few fixed processing-microstructure conditions. Most of the properties measured at temperatures up to 760°C appear to be comparable to, or better than, those of the counterpart Ni-base superalloys when adjusted for density [Ref. 8]. These desirable material properties include stiffness, high temperature strength, creep, oxidation resistance, and corrosion resistance. Fatigue crack growth, impact resistance, and ductility have been items of concern, however, and appropriate measures are needed in engineering design stages, as well as during handling and fabrication processes, to accommodate such deficiencies. [Ref. 2]

B. POTENTIAL APPLICATIONS OF GAMMA-TiAl ALLOYS

The density of gamma components is approximately half of that for the nickel-based superalloys or stainless steel. This factor gives gamma alloys a significant advantage in aerospace and automotive applications because a material with low density reduces the centrifugal stresses in rotating machinery and keeps the weight of those rotating components low.

The largest anticipated usage of gamma alloys is in aircraft gas turbines as turbine blading. The turbine blade must have sufficient ductility to handle stress concentrations of operation, and must also have good resistance to oxidation and hot corrosion since the turbine blade is exposed to a high temperature, highly oxygenated atmosphere with corrosive products of combustion also present.

Resistance to creep at high temperatures is also important because minimum tolerances between the turbine blade shroud and casing are essential for maximum efficiency and performance.

Gamma components for gas turbine engines have been identified for rotational parts such as low pressure turbine (LPT), high pressure compressor (HPC) blades, and high pressure turbine (HPT) blade cover plates, and stationary parts, such as transition duct beams, vanes, swirlers, various cases, and nozzle flaps and tiles [Ref. 8]. For the past few years, the data bases and damage tolerance of various gamma alloys have been assessed for some of the identified components, through various qualification tests including bench tests, rig tests and engine tests, by several companies, including GE, P&W, MTU, Rolls Royce, and IHI. [Ref. 2]

Perhaps the most significant qualification tests were the rigorous engine tests conducted in 1993 and 1994 by GE on a full set wheel of 98 LPT cast gamma blades made of Ti-47Al-2Cr-2Nb [Ref. 9]. The two successful engine tests involving over 1500 simulated flight cycles were a milestone for the gamma alloy. Through these and other tests, the cast gamma alloys are proving to be technologically sound materials and, with some design modifications pertinent to each component, can replace nickel-based superalloys in use for the type of engine components mentioned earlier, as well as other components. Accelerated uses of gamma alloys in replacing the current materials are expected to be realized when many uncertainties about the performance in the field are cleared up or answered and low cost manufacturing processes are demonstrated for important types of components. [Ref. 2]

Cast TiAl alloys are also intended for use in automotive engine parts such as turbochargers and valves. Recent engine tests show that a cast TiAl turbocharger rotor exhibits better acceleration response and higher maximum rotational speed than its counterpart, Inconel rotor [Ref. 10]. Exhaust engine valves appear to be an ideal application for gamma alloys, which are expected to replace the current valves made of steel and /or nickel-base (Inconel) alloys. The properties of gamma alloys in many microstructural forms well exceed most of the property requirements, as was evaluated and demonstrated through a series of extensive qualification engine tests conducted at GM [Ref. 11]. The remaining barrier appears to be development of a low-cost, high volume manufacturing method. Intensive production and alloy modification efforts to reduce the cost are underway worldwide. [Ref. 2]

C. OBSTACLES TO DEVELOPMENT AND APPLICATION

1. Establishing Phase Diagrams

The binary Ti-Al phase diagram is shown in Figure 2.1. The central portion of the Ti-Al phase diagram was controversial for nearly 40 years, as indicated by the dashed lines in Figure 2.1, before the currently accepted version was constructed. This version, as depicted in Figure 2.2, shows three solid phases (γ-TiAl, α_2-Ti_3Al, and high-temperature α-Ti) and two-phase reactions (a peritectic $L+\alpha \rightarrow \gamma$ reaction and a eutectoid $\alpha \rightarrow \alpha+\gamma$ reaction) [Ref. 14]. Investigation is still in progress as to the exact location of some phase boundaries, but from the binary phase diagram, some additional features should be noted.

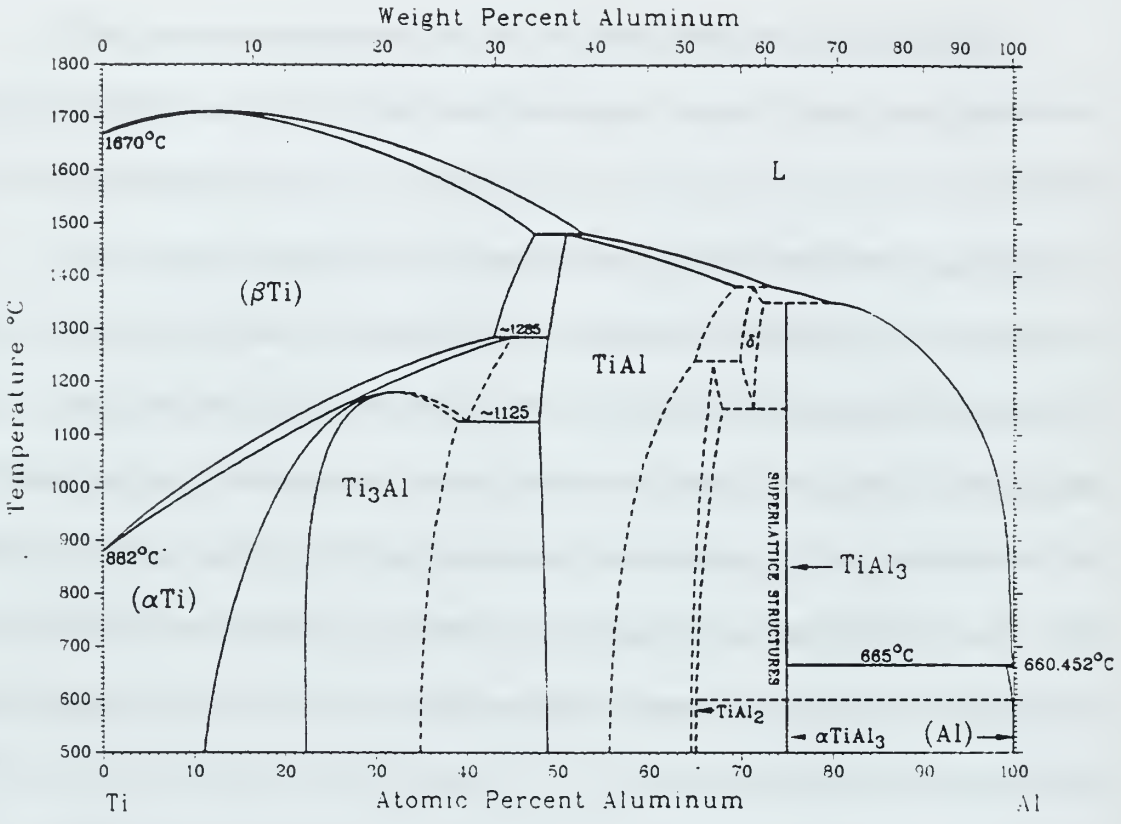

Figure 2.1 Binary TiAl Phase Diagram [From Ref. 12]

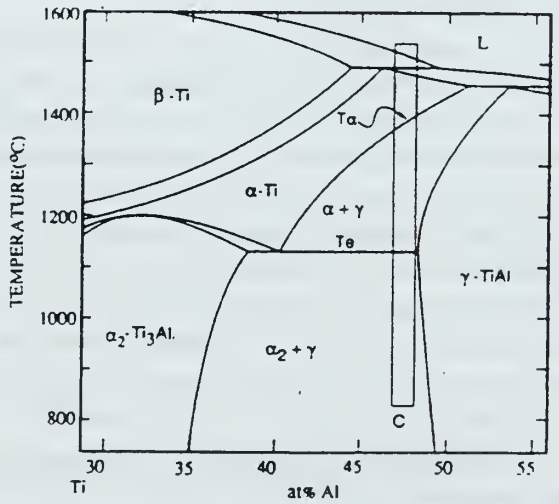

Figure 2.2 Central Portion of Binary TiAl Phase Diagram [From Ref. 13]

The α_2-Ti_3Al phase is an ordered hexagonal close packed (h.c.p.) structure with the Strukturbericht designation $D0_{19}$, and remains ordered up to 1150°C. It has a composition that can vary between 22 at.% and 39 at.% aluminum depending on temperature. The γ-TiAl phase with the $L1_0$ (ordered face centered tetragonal (f.c.t.)) structure has a composition that varies between 48.5 at.% and 66 at.% aluminum depending on temperature, and it remains ordered up to its melting point of ~1450°C. For the stoichiometric TiAl, c/a = 1.015, but this ratio varies between 1.03 and 1.01 with increasing or decreasing Al content. The third of the three intermetallic compounds titanium forms with aluminum is $TiAl_3$, which is an ordered face centered cubic (f.c.c.) crystal structure with the $D0_{22}$ Strukturbericht designation. The composition of $TiAl_3$ is stoichiometric with 75 at.% Al. The maximum solubility of titanium in aluminum is approximately 0.7 at.%. [Ref. 13]

An additional study of the binary Ti-Al phase diagram by Veeraraghavan *et al.*, [Ref. 15] indicated that the commonly accepted diagram was accurate, except for minor modifications between 25 at.% and 43 at.% aluminum.

Ternary phase diagrams have been produced for several Ti-Al-x systems, of which the Ti-Al-Nb system has been given the most extensive investigation. As illustrated by Figure 2.3, however, additional research is necessary to place phase boundaries precisely.

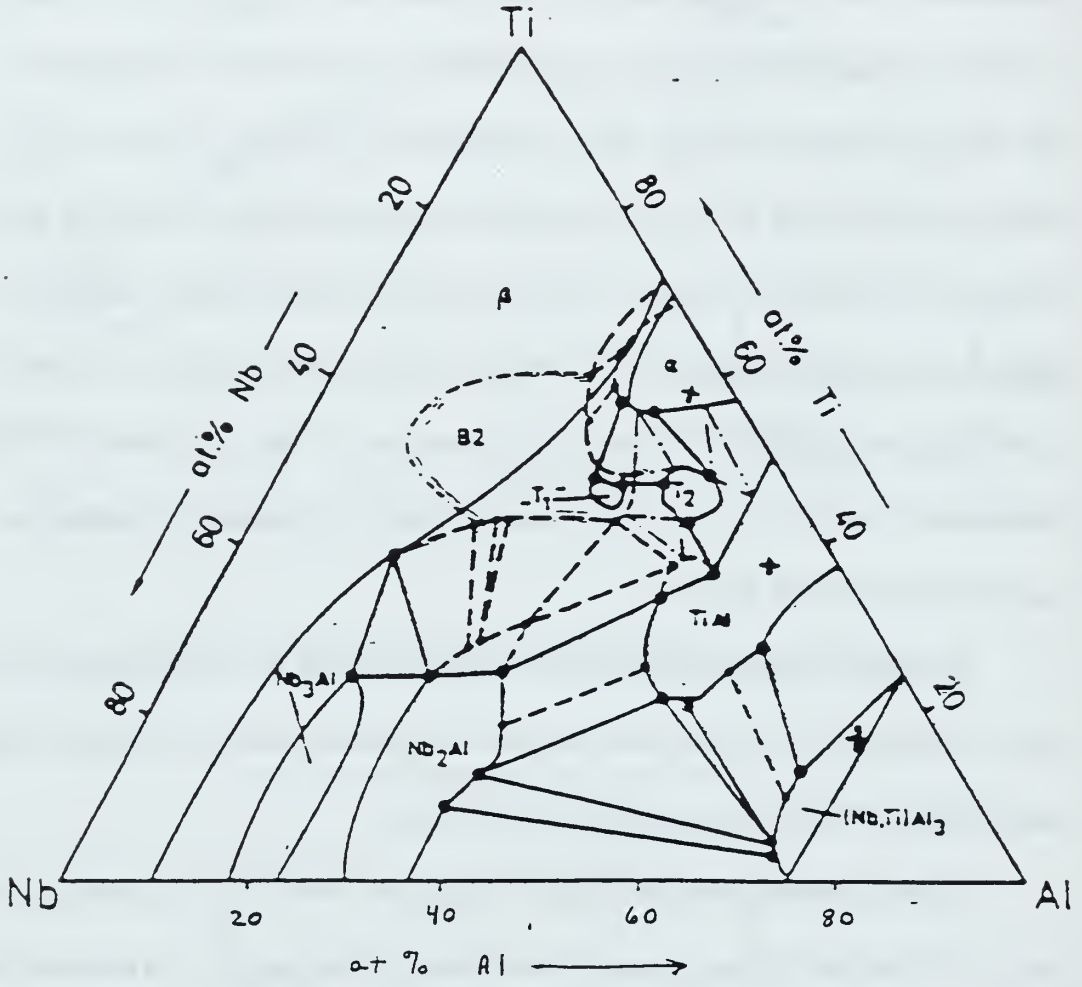

Figure 2.3 Ternary Ti-Al-Nb Phase Diagram [From Ref. 16]

2. Control of Microstructure

With the establishment of the TiAl binary phase diagram, it was possible to understand the transformations between phases, and to develop techniques to consistently produce desired microstructures. Four different types of standard microstructures have been identified: near-gamma, duplex, nearly lamellar (NL), and fully lamellar (FL) [Refs. 6, 8, 13]. Duplex and FL microstructures have been investigated to the greatest extent of the four types. A number of mechanical property measurements and evaluations have been conducted on these microstructures. In general, FL microstructures are two-phase ($\alpha_2+\gamma$) and consist of large lamellar grains resulting in poor tensile properties. Duplex microstructures are single phase (γ) and consist of fine grains, and therefore have lower fracture toughness, lower strength, and poorer resistance to creep in comparison to the other microstructural forms of gamma alloys [Ref. 8]. Understanding the behavior and failure of the alloy in its various microstructural forms is fundamental to its application in engineering design. It is impossible to design with a new material until its chemistry can be consistently controlled and the manufacturing capability exists to produce a variety of shapes that possess the desired properties and microstructure. [Ref. 2]

The near-gamma microstructures with maximum elongation are found at a composition of around Ti-48Al, and are obtained by an annealing heat treatment at temperatures just above the eutectoid temperature. (See Figure 2.2) This microstructure is generally non-uniform, consisting of course gamma grains and stringers of fine gamma grains pinned by alpha-2 particles. [Ref. 13]

The duplex microstructure is typically the finest microstructure and is produced after annealing treatments at temperatures where gamma and alpha phases are approximately equal by volume. The existing alpha-2 particles and freshly nucleated alpha precipitates coarsen into alpha plates and alpha grains. At the same time, the initially predominant gamma phase existing in hot-worked material is reduced in volume by dissolution until the equilibrium volume fraction is reached, typically in about two hours. This leads to competitive growth between the alpha phase and the gamma phase, which saturates after about four hours, resulting in a fine mixture of two-phase grains. [Ref. 13]

The nearly lamellar microstructures are produced by heat treatments at temperatures near the alpha-transus temperature ($T\alpha$) for approximately one hour. (Figure 2.2) The microstructure produced is predominantly coarse, lamellar grains with the remainder being fine gamma grains. [Ref. 13]

The fully lamellar microstructures are produced by heat treatments at temperatures above the alpha-transus temperature for as short as 10 minutes, and consist of relatively large, fully lamellar grains. [Ref. 13].

3. Fracture Resistance

Duplex microstructures exhibit small plastic strain near the onset of crack extension and no resistance to crack propagation. The fully lamellar structure, on the other hand, yields large crack-tip plastic strains and increased resistance to crack propagation [Refs. 17, 18]. The occurrence of crack growth resistance is caused mainly by the redundant work expended in failing ligaments formed in the wake of the crack. The

absence of crack growth resistance behavior in duplex structures is due to lack of bridging ligaments. Fracture toughness increases with temperature at varying rates depending on microstructure and loading rate and its sensitivity to loading rate increases with temperature [Ref. 19]. Fine grain microstructures yield improved tensile properties but low fracture toughness, and the reverse is true for large grain FL material. This relation is explained by correlating grain size, dislocation density, and the deformation anisotropy of the lamellar structure [Refs. 8, 17,20,21]. The toughness increases with decreasing lamellar spacing in fully lamellar materials having grains larger than the plastic zone size. When the grain size is smaller than the plastic zone size, then the grain boundary effect has more influence than the lamellar spacing effect on the fracture toughness. [Ref. 2]

4. Creep Resistance

Creep resistance of two-phase gamma alloys is higher for fully lamellar than for duplex microstructures and appears to increase with grain size [Ref. 8]. Creep rupture life in FL structures is increased by a serrated grain boundary morphology [Ref. 22] and perhaps by refined lamellar spacing. The presence of the gamma phase in the lamellar grain boundary regions may promote creep rates. The superior creep resistance for lamellar structures has been explained in terms of composite-like strengthening in that alpha-2 plates act as reinforcements [Ref. 23]. However, the fundamental mechanisms are unknown for the most part. The creep rupture strength depends on microstructure and test temperature. At higher temperatures, the duplex structured material is least creep

resistant. The rupture life can be extended by reducing the harshness of the environment or by using protective coatings. [Ref. 2]

5. Fatigue Resistance

High cycle fatigue behavior in gamma alloys is a function of microstructure, component geometry and temperature. Fatigue testing has indicated that the fatigue strength for both duplex and fully lamellar microstructures is up to 0.96 of ultimate tensile strength at 10^7 cycles for temperatures up to 600°C [Refs. 24, 25]. At 800°C or higher, the fatigue resistance for fully lamellar materials is much higher than it is for duplex materials. The fatigue deformation is planar and interlamellar, and the failure modes are predominantly transgranular at room temperature, and increasingly intergranular as temperature increases with lamellar splitting becoming important [Ref. 24]. Cracking generally initiates at the material surface for duplex structure and in the interior for fully lamellar materials. The fatigue crack growth rates in fully lamellar microstructures are considerably slower than those of duplex microstructures at room temperature, as well as at elevated temperatures. These rates vary depending on composition, microstructure and testing conditions, and they are strongly dependent on lamellar orientation in cast alloys [Refs. 8, 26]. Nevertheless, the improvements of the fatigue crack growth resistance in lamellar materials over duplex materials are real, which are similar to those for fracture toughness and creep resistance. [Ref. 2]

6. Use of Gamma TiAl at High Temperatures

The application of gamma TiAl alloys in operating conditions up to 850°C, or even higher, could be possible and very profitable with improved processing techniques, new alloying methods, or protective surface treatments, or a combination of the three. Some novel processing methods currently being explored are aimed at producing material having aligned lamellar structures by directional solidification of columnar grains and/or directional extrusion of lamellar grains. These methods are the subject of significant investigation for both Ni and Ti based alloys. Once the processes have been proven to produce the intended microstructures, the resulting materials must demonstrate the anticipated higher temperature capabilities as well as damage tolerance comparable to the current gamma alloys. [Ref. 2]

Achieving significant increases in high temperature strength and oxidation resistance may also be possible with significant changes in alloy composition and modifications for enhancing the interfacial boundary bond strength. Another potential method of improving creep resistance at higher temperatures is addition of a protecting oxide layer such as Al_2O_3. These methods are still in the research stage, although some advancements have been made. Some progress has been made in refining cast TiAl microstructure through the development of novel heat treatment cycles, but there appears to be a limit to the improvement in material properties possible with only microstructural control. Therefore, alloying TiAl with additional elements, new processing methods and the development of protective coatings that will maintain adhesion in extreme

environments seem to hold the most promise for dramatic improvements in possible high temperature use of gamma TiAl alloys.

D. EFFECTS OF ALLOYING

Titanium is ductile in pure form, but when alloyed with more than 6 wt.% aluminum, its hardness and brittleness increase dramatically, and continue to increase with increasing Al content. The physical metallurgy and alloying behavior of titanium is rather complex due to its allotropy, involving the h.c.p. crystal structure (α) below 882.5°C and a b.c.c. crystal structure (β) above this temperature. Alloying elements may dissolve preferentially in α-titanium (α-stabilizers), in β-titanium (β-stabilizers) or in both (neutral), thereby increasing the stability range of these phases. They may also form stoichiometric compounds with titanium. As a result, titanium alloys are classified as α-alloys (predominantly α-phase), β-alloys, γ-alloys, and so on, each group having its own characteristic properties. Alpha and near alpha titanium alloys have very good creep resistance, high strength and good weldability, but are brittle at room temperature when alloyed with aluminum. Beta titanium alloys have poor creep resistance, but good workability and formability. [Refs. 27, 28]

The intermetallic compound γ-TiAl has a low density of 3.76 g/cm^3, good resistance to oxidation and a relatively high modulus of elasticity. Like Ti_3Al, TiAl is also brittle at room temperature. The ductility of gamma alloys is controlled by alloy chemistry and microstructure. Research on Ti-(43-55)Al compositions has shown that the lowest

strength occurs at compositions around Ti-51Al [Ref. 14] and that room temperature elongation varies with Al content, with the optimum composition being Ti-48Al. This best ductility composition was believed to be due to an optimum volume ratio of the phases alpha-2 and gamma of 3-15%. Below this ratio, the grain growth becomes pronounced when heat treated in the $\alpha+\gamma$ phase field. Above this ratio, the brittle alpha-2 phase reduces the benefit of microstructural refinement. [Ref. 13]

Adding vanadium, chromium or manganese strengthens the alloys by solid solution strengthening mechanisms and increases the ductility of two-phase TiAl alloys, but has little or no effect on single-phase alloys containing more than 50 at.% Al [Ref. 5]. Chromium provides the most strengthening effect of the three elements and manganese the least. Addition of these three elements has also been shown to increase both slip and twinning activity in duplex gamma alloys [Ref. 29], but typically causes a decrease in oxidation resistance [Ref. 30]. Consequently, ductile gamma alloys with vanadium, chromium, or manganese require the addition of an element to improve oxidation resistance, such as niobium, tantalum, or silver. [Ref. 13]

Numerous studies have focused on improving the ambient temperature properties of titanium aluminides by the addition of beta stabilizers such as Ru, Mo, Nb, V, and W [Refs. 27, 28, 31-34]. These elements stabilize the body-centered cubic β-titanium at low temperatures, forming alloys with improved low temperature ductility and structures consisting of aluminide + β. The presence of significant amounts of β-Ti degrades the creep resistance and increases the overall density due to the added beta stabilizers. Martin

et. al. [Ref. 31] showed that in Ti-49Al-2W, structural refinement caused appreciable strengthening to occur without significantly decreasing the ductility, and that the high strength conditions also had improved creep resistance.

Singh and Banerjee [Refs. 32,33] conducted a study with titanium aluminide alloys containing molybdenum in a program to explore a class of alloys containing three-phase structures of alpha-2, gamma and beta. The program was inspired by the known beneficial effect of the B2 phase on the ambient temperature ductility, toughness and high temperature strength of Ti_3Al-based alloys. Their first study was conducted with molybdenum, which is one of the strongest beta stabilizers.

Kawabata, et. al. [Ref. 34] conducted a study to investigate the effect of ternary additions of V, Cu, Nb, Zr, and Mn on mechanical properties of TiAl at room temperature, 873K and 1073K. It was determined that the vanadium addition increased yield and fracture stresses at all test temperatures, but did not change the fracture strain for the tested composition. The addition of copper resulted in slight improvements in strength and ductility at 1 at.% but decreased the fracture stress and strain at 2 and 3 at.%. The addition of 2 at.% niobium slightly increased yield and fracture stresses and caused a large increase of fracture strain at 873K. The zirconium addition resulted in a large increase of yield stress and an increase in fracture strain at 2 at.%, but a decrease in fracture strain with increasing at.%. The addition of manganese increased the yield and fracture stresses and fracture strain at the lower two temperatures and produced a fine grain size.

E. TITANIUM-ALUMINUM-NIOBIUM ALLOYS

These studies serve to indicate that gamma titanium aluminum in the binary condition is unsatisfactory for practical application in the desired high temperature areas. However, with additional alloying using beta stabilizers and oxidation resistance improving elements the overall performance of the resulting alloy is outstanding. Of the elements investigated, niobium is a beta stabilizer, and also improves oxidation resistance. This has provided the impetus for the extensive amount of research that has been devoted to niobium as an addition to the Ti-Al system and many of the gamma titanium aluminides in serious contention for application have at least 2 at.% Nb.

Recently, a great amount of work has been directed at thermomechanical processing and control of microstructure in an attempt to overcome the material's shortcomings at high temperatures, as well as ambient temperature ductility. Evidence now indicates that major improvements in properties will not be achieved by relatively small amounts of alloying elements, and that additions greater than 5 at.% will be necessary. [Refs. 13, 35]

Research efforts are concentrating on titanium aluminides with higher percentages of niobium and the current literature provides a better understanding of the ternary phase system and transformations and deformation behavior. Cheng and Loretto [Ref. 35] studied the decomposition of the beta phase in alloys containing niobium concentrations of 4 and 8 at.% and produced a schematic Continuous Cooling Transformation diagram from the results. Yu and Koo [Ref. 36] conducted a phase characterization of a hot-rolled Ti-

40Al-10Nb alloy and reported the phases observed to further define the ternary phase diagram at the 1000°C, 1100°C, and 1200°C isotherms.

Of particular interest to our study at the Naval Postgraduate School are the results produced by Wang, et. al. [Ref. 37] and Paul, et. al. [Ref. 38] because one alloy used in both studies was Ti-45Al-10Nb, which is very similar to the Ti-44Al-11Nb alloy used in our investigation.

Wang et. al. [Ref. 37] conducted TEM studies of mechanical twins in the alloy in a hot-deformed condition to determine possible dislocation mechanisms. Earlier work by that group had shown Ti-45Al-10Nb to be a high performance alloy with excellent high temperature strength and oxidation resistance. By adding 10 at.% niobium, the stacking fault energy was decreased, and twinning and twin intersection were enhanced.

Paul et. al. [Ref. 38] studied the compression behavior of the Ti-45Al-10Nb alloy and two other ternary alloys containing higher percentages of niobium, as well as three binary TiAl alloys. The binary alloys had comparable percentages of aluminum to the ternary alloys when niobium is assumed to preferentially occupy Ti lattice sites. Previous investigations using the ALCHEMI method have revealed that niobium has a nearly 100% probability of occupying titanium sites when added to TiAl [Refs. 39-41]. Considering that proof, Paul's group concluded that by comparing the properties of the niobium containing alloys with the binary alloys, the high strength of the ternary alloys was solely a result of the reduced aluminum content, and that niobium plays no role in strengthening or work hardening. However, the potential beneficial effect of niobium on ductility of gamma-TiAl was not part of the investigation.

F. DIRECTIONAL SOLIDIFICATION PROCESSING

The use of alloying elements is one approach to produce a desired microstructure and thereby achieve a balance of mechanical properties such as tensile strength, fracture toughness and ambient temperature ductility. Another approach is to use directional solidification processing to create an oriented lamellar structure. When the lamellar boundaries are parallel to the tensile axis, tensile ductility and yield stress are optimized. If a directionally solidified microstructure composed of columnar grains in the lamellar form is produced, with the growth direction parallel to the lamellar boundaries, there is potential for significant improvement in strength, ductility and toughness over non-aligned structures. [Ref. 42]

For two-phase gamma alloys with fully lamellar structures, this processing method uses the anisotropic nature of the lamellar microstructure to advantage. When the growth direction and lamellar orientation are parallel, the combination of strength and toughness would be optimized. The microstructure would consist of columnar grains oriented in the growth direction, as indicated in Figure 2.4. When a material with such a structure is tested in uniaxial tension in the direction of grain growth, the columnar grains are believed to deform macroscopically in an anisotropic manner such that deformation perpendicular to the tensile axis is negligible. This anisotropic deformation may cause incompatibilities between adjacent grains and negatively impact ductility, however, this will positively affect strength, and a reasonable amount of ductility is still expected. [Ref. 42]

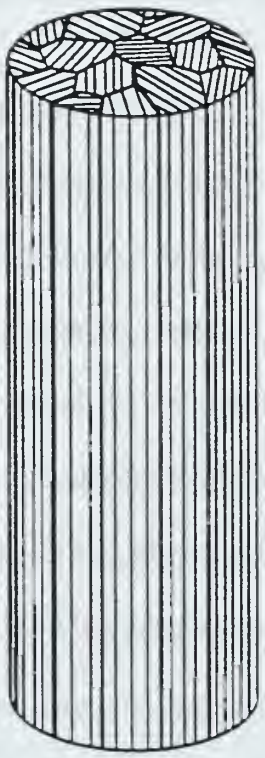

Figure 2.4 Directionally solidified structure of columnar grains [From Ref. 42]

There are two ways to control the lamellar boundary direction in directional solidification processes. One is using a seed crystal, and the other is modifying the solidification procedure [Ref. 43]. To control the lamellar orientation using a seed crystal, the alpha phase must be stable from melting temperature to room temperature because the lamellar microstructure is not formed in the liquid state during solidification, but rather in the solid state. This procedure is described in three papers by Johnson et al. [Refs. 44-46]. Figure 2.5 shows a schematic of a possible growth morphology that may occur during directional solidification.

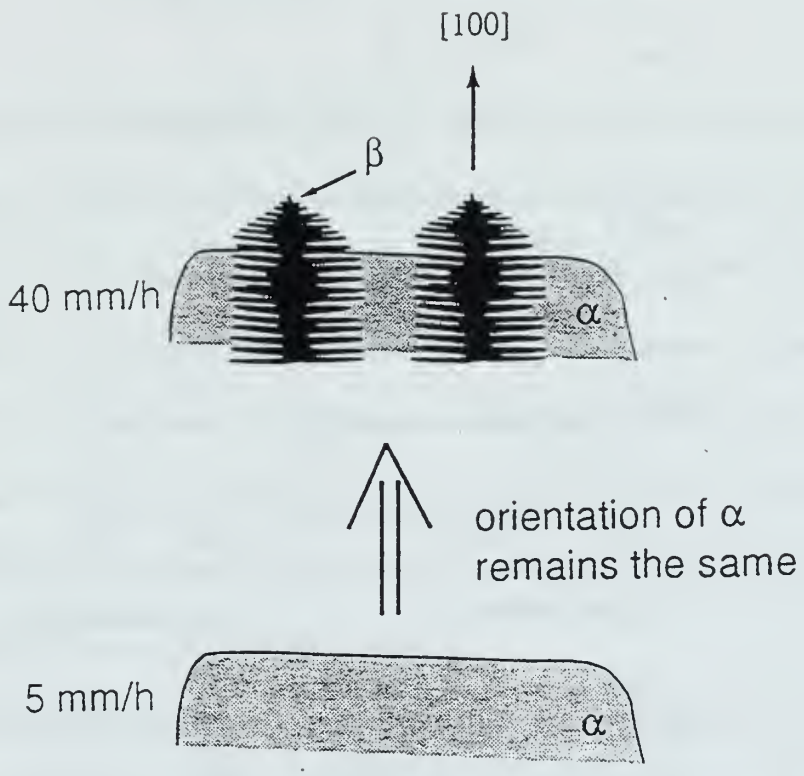

Figure 2.5 Possible growth morphology for directional solidification. [From Ref. 46]

In the modifying solidification procedure, the only requirement is full transformation to the beta phase from the liquid upon cooling. To obtain fully lamellar structures aligned with the growth direction, the alloy composition was shifted to aluminum compositions of less than 45 at.% Al. The advantages of the modifying solidification procedure and the process itself are described in Kim et al. [Ref. 43], along with the results of their investigation of the effects of alloy compositions and growth rates on the microstructure and deformation behavior of fully lamellar TiAl alloys. Figure 2.6 shows the solidification procedure for two different compositions of a binary TiAl alloy.

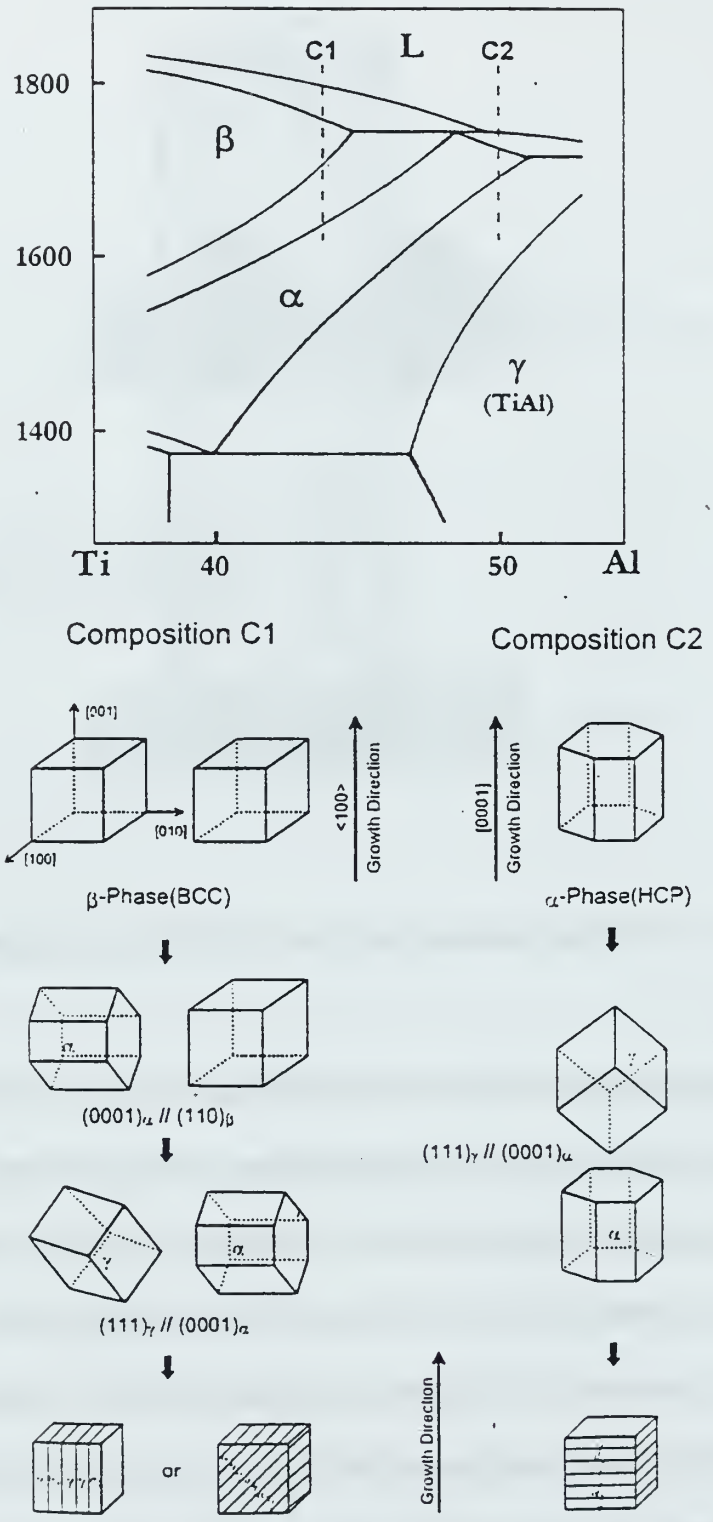

Figure 2.6 Solidification procedure for compositions C1 and C2. [From Ref. 43]

III. SCOPE OF THE PRESENT WORK

The previous discussion has shown the need for improvement on present-day alloys for high temperature applications and the gamma titanium aluminides hold excellent potential for service in those conditions. The addition of large amounts of niobium as an alloying agent to potentially improve strength, ductility and oxidation resistance is a recent development and as the literature has indicated, not all results are in agreement concerning the properties of these alloys. Clearly much more research is needed to establish the ternary phase diagram and understand the nature of the phase transformations involved, as well as resolve differences in investigative results.

The directional solidification process promises excellent benefits in designing materials with optimum mechanical properties for use in high temperature applications. Research in the use of directional solidification processing with gamma titanium aluminides has not occurred until relatively recently.

It would appear that there is significant potential in pursuing both alloying with large amounts of niobium and directional solidification to produce an alloy that possesses the highly desirable characteristics of low density, good high temperature strength and stiffness, good thermal expansion, good oxidation resistance, and hot corrosion resistance, as well as creep resistance, impact resistance, and room temperature ductility. This study will look at a gamma TiAl alloy with 11 at.% niobium that has been directionally solidified and compare it with an as-cast sample of the same composition.

Research to date at the Naval Postgraduate School has been in the binary gamma-TiAl alloys with a study of the Debye-Waller factors of stoichiometric and Al-rich γ-TiAl alloys [Ref. 47] and two Master's theses.

The objective of the current investigation is to characterize the microstructural development of a Ti-44Al-11Nb alloy as a means to determine the cause of its demonstrated improved ductility compared to the more brittle gamma-TiAl. This will involve preparing samples of chill-cast and directionally solidified Ti-44Al-11Nb, identifying the phases present in each sample by x-ray diffraction, and studying the microstructures by optical and electron microscopy methods. The elemental and phase distributions will be studied with advanced transmission electron microscopy techniques including energy dispersive x-ray (EDX) spectroscopy and spectrum imaging.

IV. EXPERIMENTAL METHODS

A. METAL BUTTON INGOT FABRICATION

Specimens of Ti-44Al-11Nb alloy for this study were provided by Dr. Rabin Mahapatra of the Naval Air Warfare Center, Patuxent River, MD.

1. Chill-Cast

The tested alloy with a nominal composition of 45 at.% Ti, 44 at.% Al and 11 at.% Nb was prepared as a cast ingot from commercially pure elements (99.998 %) by non-consumable arc melting in a purified argon atmosphere at 1 atm. During melting the buttons were turned and remelted at least three times to promote homogeneity and then cooled in the argon atmosphere to prevent oxidation. The final dimensions of the button ingot were approximately 20 mm in diameter and 10 mm in thickness.

2. Directionally Solidified

The button ingot was prepared as described above. The arc-melted button was then remelted in an arc furnace to produce rods 10 mm in diameter and 80 mm long. The rods were turned over and remelted at least 2 times in the arc furnace. Directional solidification was performed in an ASGAL Optical Imaging Floating Zone Crystal Growth furnace at the University of Pennsylvania. Two 3.5 kW tungsten halogen lamps used as heat sources are enclosed in a double ellipsoid gold plated water-cooled chamber (Figure

4.1). Radiant energy emitted from the two lamps is focused onto the molten zone where the tip of the feed rod is melted and solidified onto the tip of a seed rod placed underneath. As the feed and seed rods move downward together, the molten zone passes through the feed rod, such that the crystal growth rate is 5 mm/hr. To prevent oxygen entrapment, the process is contained within a quartz tube with a purified flowing argon gas atmosphere. The growth process is monitored on a viewing screen with the working area projected through an optical system. [Ref. 48]

ASGAL Optical Imaging Floating Zone Crystal Growth Furnace.

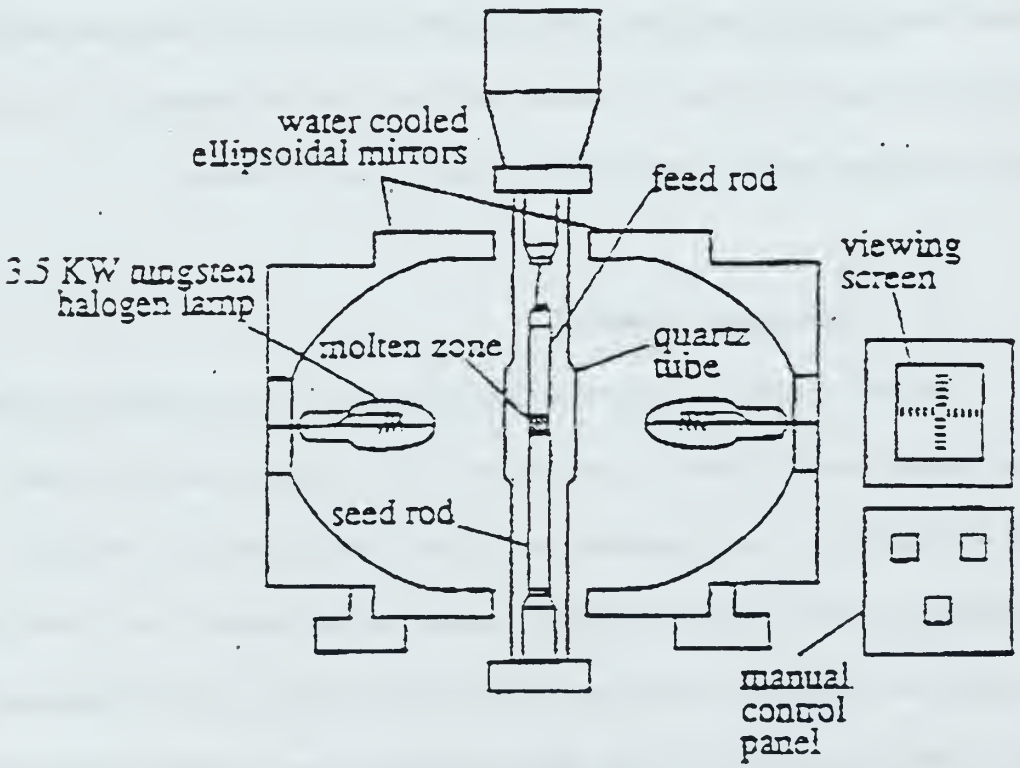

Figure 4.1 Schematic diagram of directional solidification apparatus. [From Ref. 48]

The advantages of the Optical Imaging Floating Zone technique of crystal growth is that it is containerless, which fully eliminates the possibility of interactions between a mold and the material being processed, and the resulting crystals are frequently free of porosity. This is likely due to continual filling of the voids from the liquid zone. The disadvantages are that the growth process is slow and requires constant operator supervision. Other difficulties with the procedure include the requirement to have cylindrical shaped stock material and good alignment of the seed crystal and feed rod to prevent collapse of the molten zone, as well as the small diameter and the oxygen absorption potential of the crystals produced. [Ref. 48]

B. SAMPLE PREPARATION

1. Wafer Cutting

Wafer cutting of both the chill-cast and directionally solidified samples was performed on a Buehler Isomet Low Speed Saw with a Buehler Diamond Wafering Blade (Series 20 HC Diamond) at 125-175 rpm and 25-75 g loads. The initial cutting of the chill-cast sample was across the center diameter of the button. One wafer of this cross section was cut to 1 mm thickness and used for x-ray diffraction (XRD) analysis and transmission electron microscopy (TEM) samples. One of the remaining button halves was cut in thin wafers perpendicular to the existing cut surface to expose a different face orientation. Several wafers were cut from this exposure for XRD, optical microscopy and

scanning electron microscopy (SEM). Cutting times were typically 12-24 hrs. and occasionally longer depending on the cut face dimensions.

Cutting of the directionally solidified sample was performed to expose a surface parallel to the axis of growth and another surface perpendicular to the growth direction.

Samples were mounted in pucks constructed from Buehler Conductomet powder for optical microscopy and SEM analysis.

2. Mechanical Grinding and Polishing

Grinding and polishing of samples for all analysis was conducted on Struers Knuth Rotor-3 and Buehler Ecomet 4 grinding and polishing machines at moderate speeds using 220, 320, 500, 1000, 2400, and 4000 grit waterproof silicon carbide abrasive paper. Further polishing was conducted on Buehler Ecomet 3 using Buehler Metadi Diamond Suspension 3μm and 1μm on Buehler Microcloth and Felt pads at medium to high speeds. Polishing times for the more abrasive papers were typically 10-15 min per grit size. Polishing times for the finer grit papers and the diamond suspension was up to an hour each. Excessive polishing with the colloidal diamond solution created pitting of the polished surface due to the brittle nature of the alloy. Close observation was required to identify when the maximum polishing effect was achieved and pitting began to occur.

3. Etching

Surface etching of the optical and SEM samples was conducted using a solution of 1% HF-2% HCl-97% Distilled H_2O. A cotton swap applicator was used to apply the

etchant to the sample surface. The etchant was allowed to remain on the sample surface for 15 second increments until the total time required to cause visible surface etching was determined. Total etching time was typically 2-2.5 min for ambient temperatures of 60-65°F. The etchant was diluted and removed from the sample surface with running tap water, followed by a methanol rinse and heated forced air drying.

4. TEM Foil Preparation

Samples for TEM analysis were selected from thin slices of both chill-cast and directionally solidified specimens, and 3 mm discs were cut by spark erosion. Discs were mounted on a copper block with thermowax for reduction in thickness to 50 μm by mechanical grinding and polishing. Thin foils were prepared from the discs by twin-jet electropolishing with a E.A. Fischione Model 120-230 machine using a solution containing 3 % perchloric acid, 35 % *n*-butoxyethanol and 62 % ethanol (by volume) at 75V and a temperature of 210-220K. Some difficulty was experienced in keeping the discs in the teflon holding apparatus for electropolishing. To prevent the disks from slipping in the holder, thin copper rings were placed on either side of the disc to allow electrical contact with the platinum electrode while keeping the disc centered. Polishing times varied from 15 to 30 minutes per foil.

C. X-RAY DIFFRACTION

Specimens were prepared by grinding and polishing to provide a flat surface for diffraction. X-ray diffractograms were obtained at room temperature (approx. 300K) from the specimens using a Philips PW 1830 x-ray generator, and a Philips PW 3020 powder diffractometer directed by a Digital 3100 VAX workstation with power settings of 30kV and 35mA. Measurements were made by step scanning in the 2θ angle range 10-140°, with a step size of 0.02°, and a dwell time of 15 seconds. Total run time per sample was 27 h 5 m.

The resulting intensity versus diffraction angle (2θ) data files were analyzed using the VAX workstation and the Philips APD1700 software package to compare the generated data with standard diffraction patterns for phases in the Ti-Al-Nb phase diagram, and in particular with the stoichiometric Ti_3Al, TiAl, and Al_3Ti phases.

D. OPTICAL MICROSCOPY

Specimens were mounted in Buehler Conductomet pucks for ease of surface preparation, polished and etched as described above. Visual inspection of polishing and etching progress, and optical microscopy was performed on a Zeiss Jenaphot 2000 optical photomicroscope with an attached Pulnix TMC-74 optical camera. The camera was operated with Semicaps photo analysis software on a 486/DX2 computer workstation to produce photo micrographs in digital format. Magnifications in the range of 16x to 1260x

were possible. Digital photo files were stored on optical disc for printing on the Mitsubishi CP1000u Color Video Copy Processor or insertion into text or video presentation files.

E. SCANNING ELECTRON MICROSCOPY (SEM)

Specimens mounted, polished and etched for optical microscopy were also used for scanning electron microscopy on a TOPCON SM-510 SEM with tungsten filament. This SEM is equipped with both secondary and backscattered electron detectors, an intrinsic germanium energy dispersive x-ray detector with ultrathin window, and a TEXSEM backscattered diffraction camera and computer.

The system was energized to 20 kV and used a working distance of 28 mm and spot size 10. Specimens were mounted in a standard holder with the observed surface horizontal. Analysis was performed with Oxford Link Isis (Rev 3.0) and Link Tetra software on a Hewlett Packard Vectra VE/486 workstation. Backscattered electron (BSE) imaging was used to record digital images, and the intrinsic Ge x-ray detector was used to conduct specimen composition analysis, and to perform qualitative linescans and elemental x-ray mapping for selected elements. Results were stored as data files or printed on either a Mitsubishi CP1000u Color Video Copy Processor or Hewlett Packard DeskJet color printer.

F. TRANSMISSION ELECTRON MICROSCOPY (TEM)

The prepared thin foils were examined using a TOPCON EM-002B transmission electron microscope (TEM) with scanning transmission (STEM) capability and a LaB_6 emitter. This TEM is equipped with an EDAX Si-Li energy dispersive x-ray (EDX) detector (ultrathin window), an EmiSpec Vision System and a GATAN PEELS imaging filter.

Using the microscope in STEM mode allows greater flexibility of the TEM because the collection angle of the detector can be adjusted, effectively creating a variable objective aperture. This gives more control over which electrons contribute to the image generated. This capability allows generation of images in the TEM that show contrast for mass and thickness, making identification of differing material compositions possible. [Ref. 49]

The EmiSpec Vision system and STEM capability were used to generate linescan EDX spectra using probe sizes ranging from 9.3 nm to 16 nm, step sizes from 10 nm to 25 nm, and collection times of 1.5 to 25 seconds per step.

Diffraction patterns are used to conduct crystallographic analysis with the TEM, allowing identification of phases in the sample. The ability to determine crystallographic orientation is a function of the TEM that is not possible with SEM or optical microscopy. The selected area diffraction (SAD) method was used in this investigation to study the crystallography of selected areas of each specimen.

V. RESULTS AND ANALYSIS

A. VISUAL INSPECTION AND INITIAL EVALUATION OF MATERIALS

1. Appearance of Coring

Upon completion of wafer cutting in the chill-cast sample, a segregation of phases was noted with three distinctly different microstructures, as shown in Figure 5.1. Analysis with x-ray diffraction (XRD) proved inconclusive, so the sample was evaluated using the scanning electron microscope (SEM) to determine the composition of each of the three areas. It was determined that incomplete melting of niobium had likely occurred during fabrication, and the segregation was due to non-uniform elemental distribution within the sample. The remaining half of the button ingot was sent out for homogenization treatment to ensure uniformity throughout the specimen before conducting further analysis.

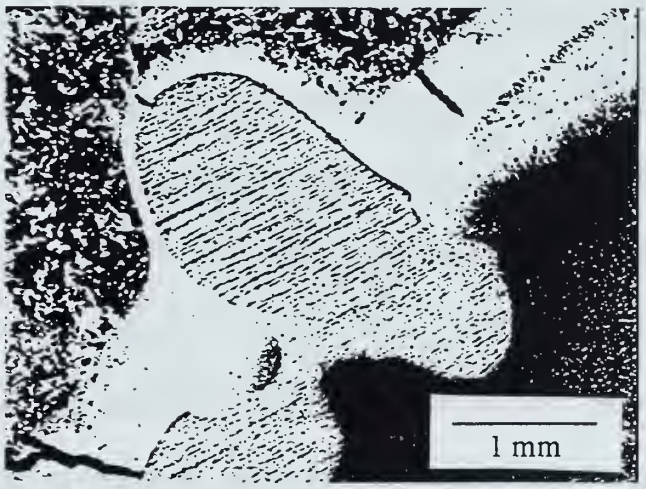

Figure 5.1 Non-uniform microstructures in Ti-44Al-11Nb (at.%) chill-cast sample

2. Homogenization of the Chill-cast Structure

The button ingot half was placed in a helium atmosphere for homogenization at 1300°C for 48 hours. Unfortunately, at that temperature, the sample separated and was deemed unusable. Another button ingot was fabricated by arc-melting and was flipped and remelted several times to ensure even mixing of elements. This button was cut in half and one half was homogenized in a helium atmosphere at 1150°C for 48 hours. The two halves of the ingot were then returned to NPS for evaluation.

It was noticed immediately that the new samples were significantly harder and much less ductile than the previous sample. Optical microscopy revealed a well-defined dendritic structure in the chill-cast section and a nearly uniform single-phase structure in the homogenized section. X-ray diffraction analysis indicated that the primary phase in both samples was γ-TiAl with Nb in solution.

The reason for the extreme hardness and brittleness of the new samples was not apparent until SEM analysis was conducted. This analysis revealed that the samples had been mixed to create Ti-44Al-11Nb by weight percentage rather than by atomic percentage. The resulting composition was approximately Ti-58.6Al-4.5Nb (at.%) which would lie toward the aluminum rich end of the gamma phase region as indicated by the phase diagrams (Figures 2.1, 2.3).

Micrographs of the Ti-58.6Al-4.5Nb (at.%) homogenized and as-cast samples obtained by SEM backscattered electron (BSE) imaging are shown in Figures 5.2 and 5.3, respectively. The homogenized structure is quite uniform, revealing little color contrast.

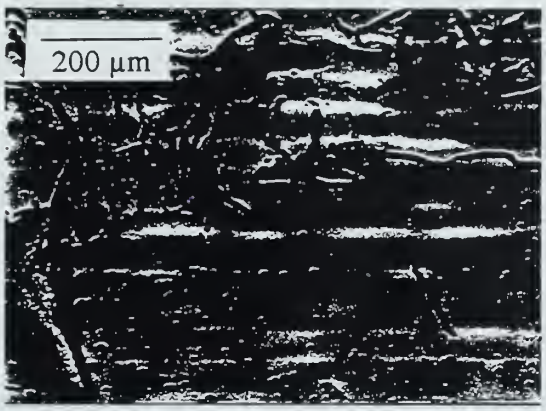

Figure 5.2 Ti-58.6Al-4.5Nb (at.%) homogenized structure

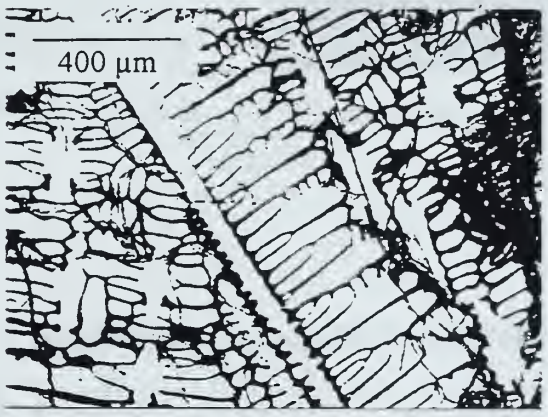

Figure 5.3 Ti-58.6Al-4.5Nb (at.%) as-cast structure

In the as-cast specimen, regions between dendrites are both Al-rich and Nb-depleted as can be seen in the qualitative elemental x-ray mapping of a dendritic region (Figure 5.4).

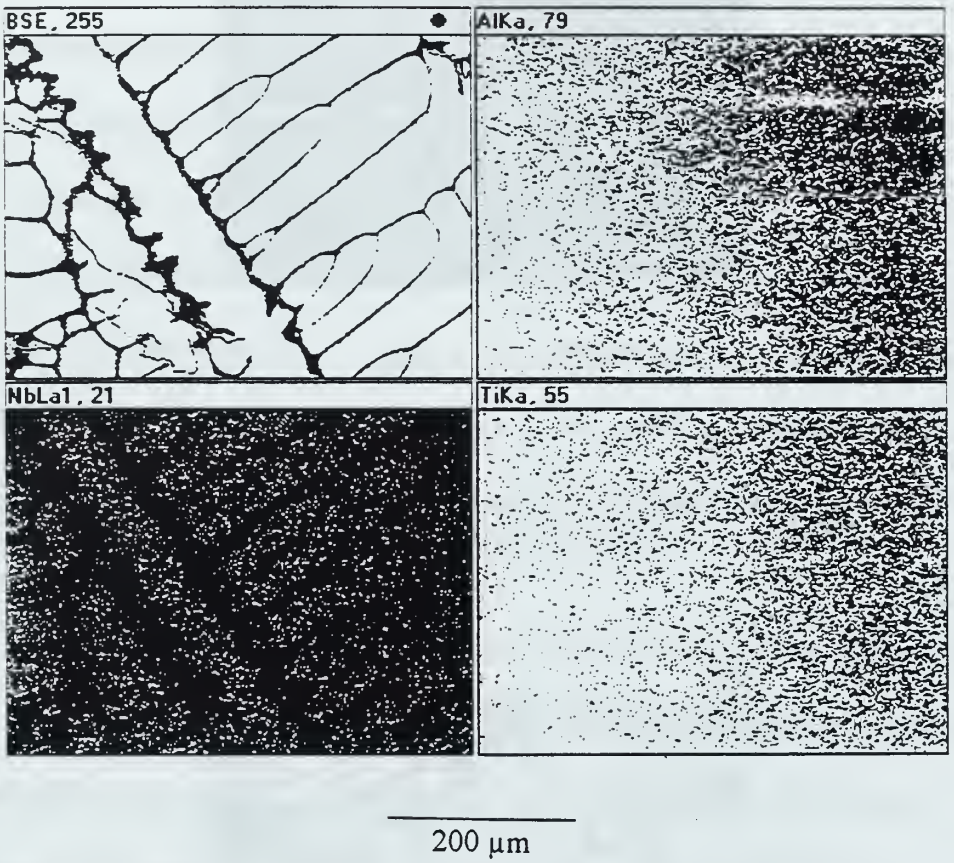

Figure 5.4 Ti-58.6Al-4.5Nb (at.%) as-cast elemental x-ray mapping

Analysis of the Ti-58.6Al-4.5Nb (at.%) alloy contributed very little valuable information to the overall study, but two aspects of the results obtained apply to the Ti-44Al-11Nb (at.%) samples:

(1) a homogenization treatment of the chill-cast structure creates a more uniform elemental distribution in a near-gamma phase
(2) increasing the aluminum content reduces ductility

All remaining discussions in this thesis will be restricted to the Ti-44Al-11Nb (at.%) chill-cast and directionally solidified alloys.

B. ALLOY CHEMICAL COMPOSITION

The alloy samples studied in this investigation were prepared as described in the fabrication section of the previous chapter. A quantitative chemical composition analysis was performed on both the chill-cast and directionally solidified samples by energy dispersive x-ray spectroscopy (EDX) in the SEM using the intrinsic germanium x-ray detector. X-ray spectra were collected from large areas of the cut, polished and etched surfaces and quantitative analysis of these spectra was performed. Table 5.1 shows the average alloy compositions as determined by EDX from 28 measurements of the chill-cast sample and seven measurements of the directionally solidified sample.

	Chill-Cast			*Directionally Solidified*		
Composition	*Ti*	*Al*	*Nb*	*Ti*	*Al*	*Nb*
Atomic %	47.13	43.32	9.55	45.65	42.62	11.73
Weight %	52.34	27.09	20.57	49.40	25.98	24.62
Sigma (σ) %	0.23	0.17	0.25	0.28	0.20	0.32

Table 5.1 Alloy chemical composition analysis

C. X-RAY DIFFRACTION (XRD) ANALYSIS

Analysis by x-ray diffraction revealed the presence of the phases Ti_3Al, TiAl, and $TiAl_3$, with small amounts of Nb in solution. The XRD traces showing relative intensity versus diffraction angle 2θ are shown in Figures 5.5 and 5.6 for the chill-cast and directionally solidified samples, respectively. Each trace was compared with diffraction patterns from the above three phases, as well as individual elements by selection from the computer catalog file. Diffractometer tracings and comparisons with cataloged patterns for each casting type are shown in Figures 5.7 and 5.8. The primary contribution in each tracing was from TiAl as the major phase with small contributions from the other two phases.

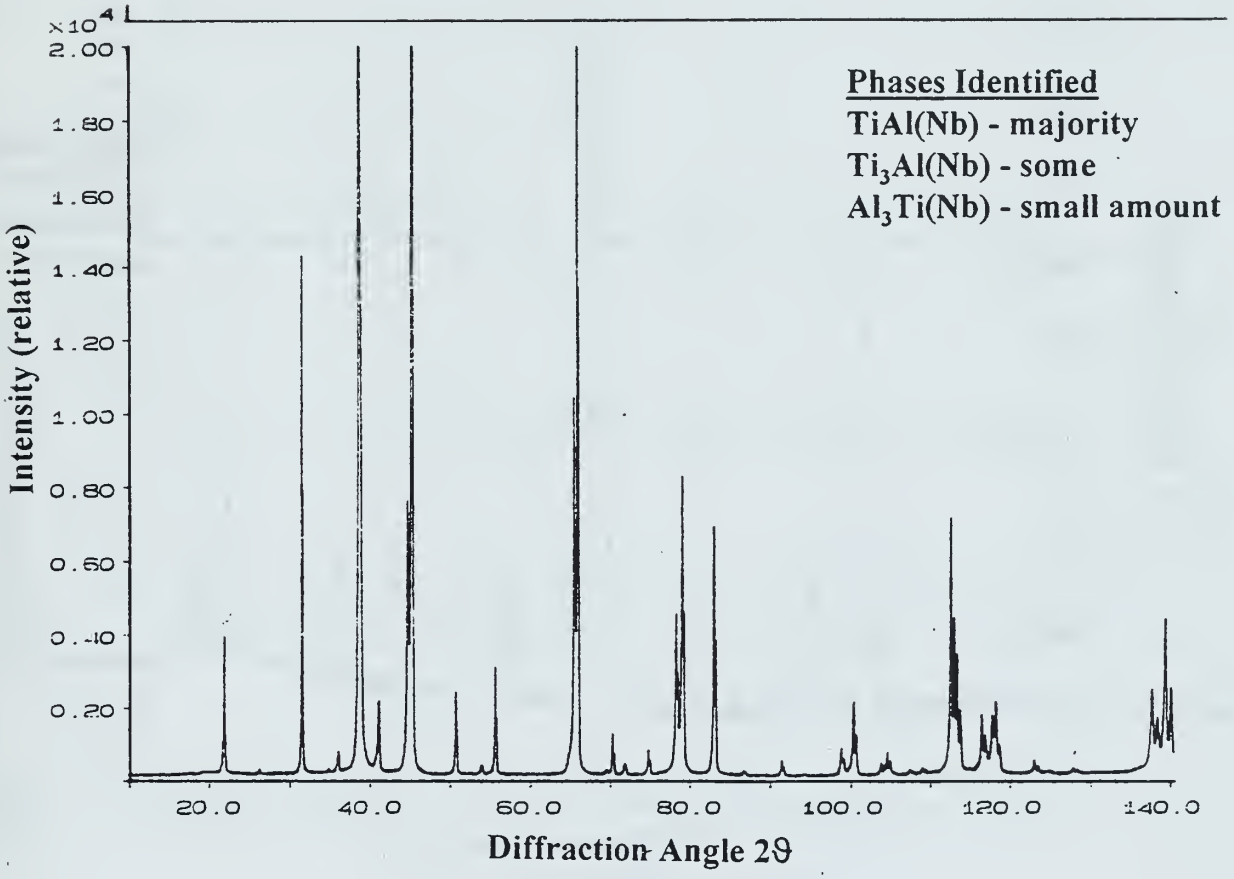

Figure 5.5 X-ray diffraction (XRD) trace for chill-cast sample

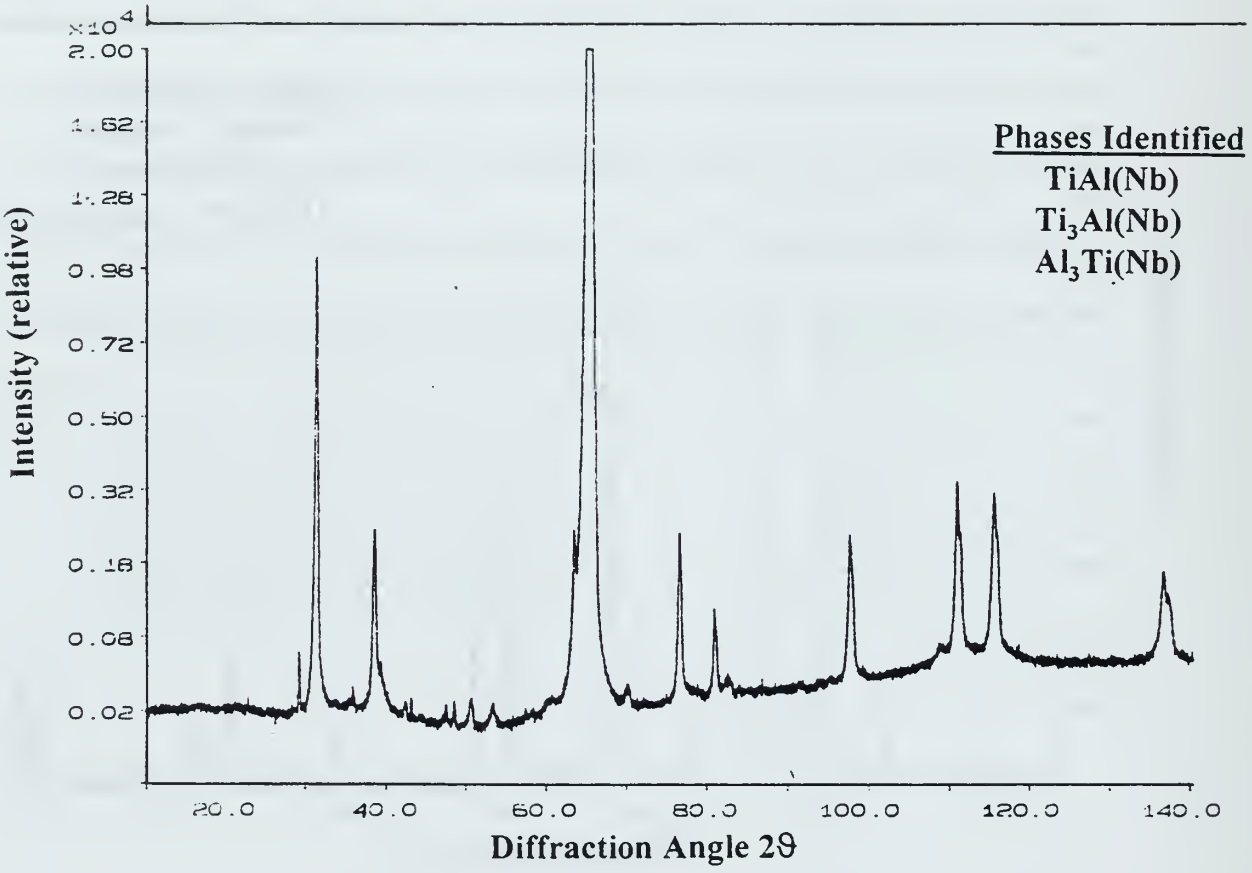

Figure 5.6 X-ray diffraction (XRD) trace for directionally solidified sample

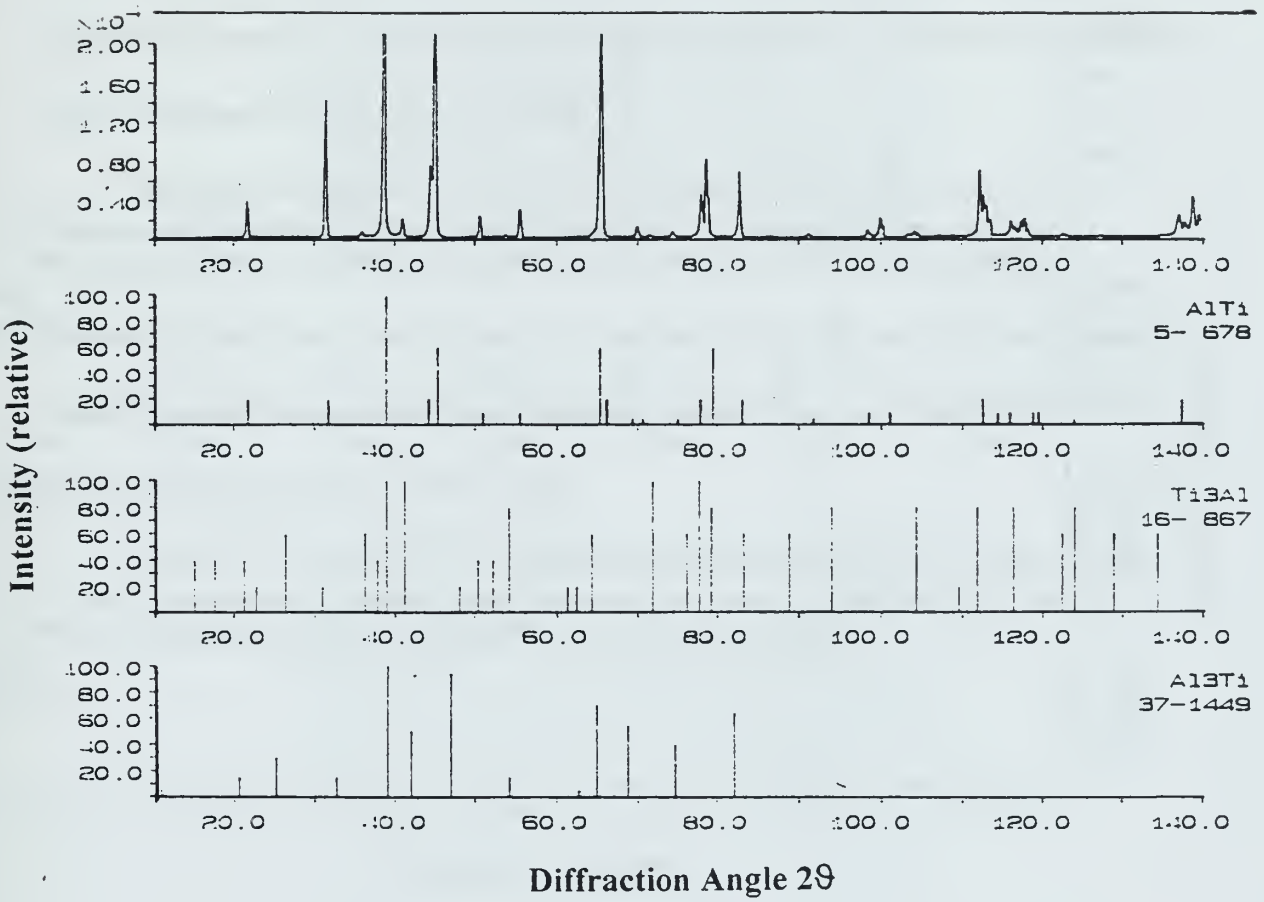

Figure 5.7 XRD comparison to reference patterns for chill-cast sample

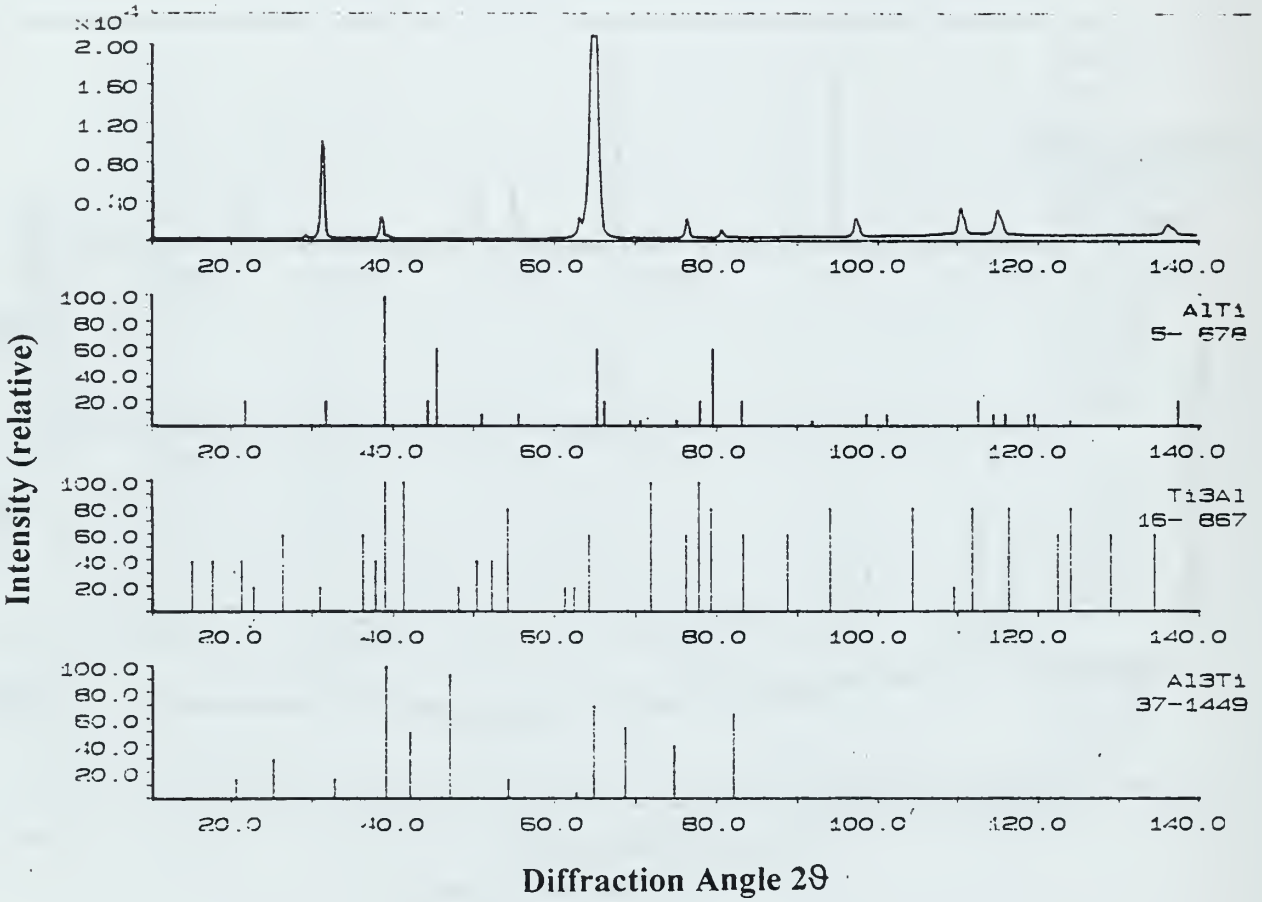

Figure 5.8 XRD comparison to reference patterns for directionally solidified sample

D. OPTICAL MICROSCOPY

Observations of polished and etched specimens revealed significantly different microstructure. The chill-cast sample grain size varied from over 200 μm in areas near the sample edge to less than 50 μm in the interior of the sample. The microstructures observed varied from grain to grain and included near-gamma, duplex, nearly lamellar and fully lamellar structures. Lamellar thickness and separation also varied widely, both within a single grain and from one grain to another.

The directionally solidified sample showed a dendritic formation on the macroscopic level, with large fully lamellar grains separated by single-phase regions. Lamellar thickness and separation were very uniform both within each grain and from one grain to the next. Grain boundaries were the single-phase regions and orientation of the parallel lamellae varied from grain to grain.

Figures 5.9 through 5.14 show photomicrographs comparing the structures of the two casting techniques at low, medium and high magnifications.

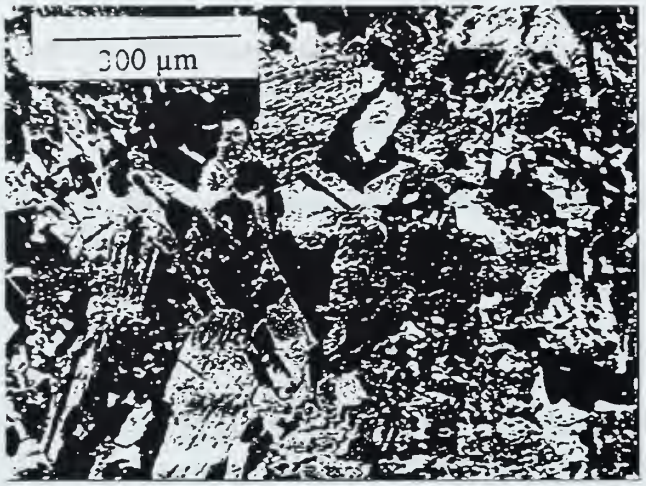

Figure 5.9 Optical micrograph of chill-cast sample at low magnification

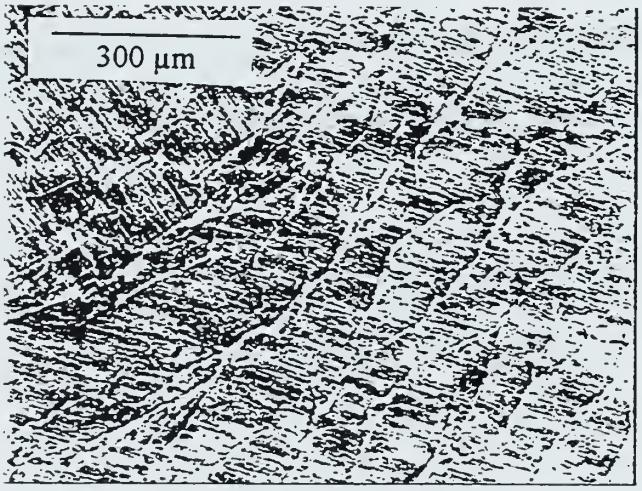

Figure 5.10 Optical micrograph of directionally solidified sample at low magnification

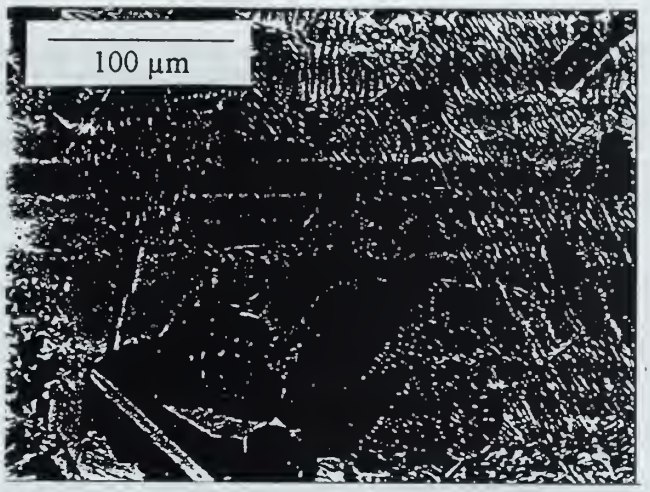

Figure 5.11 Optical micrograph of chill-cast sample at medium magnification

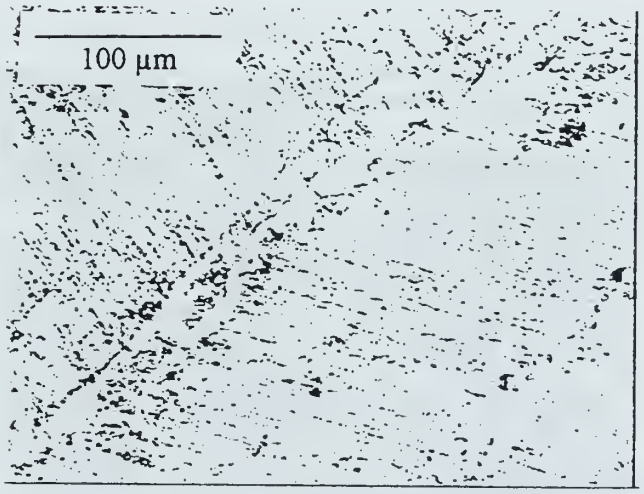

Figure 5.12 Optical micrograph of directionally solidified sample at med. magnification

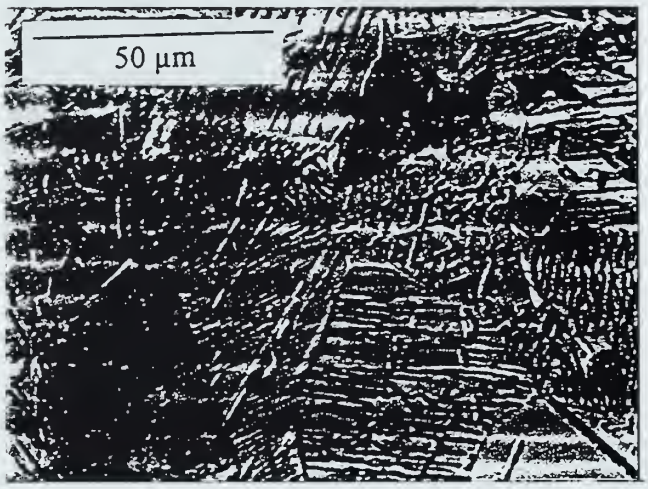

Figure 5.13 Optical micrograph of chill-cast sample at high magnification

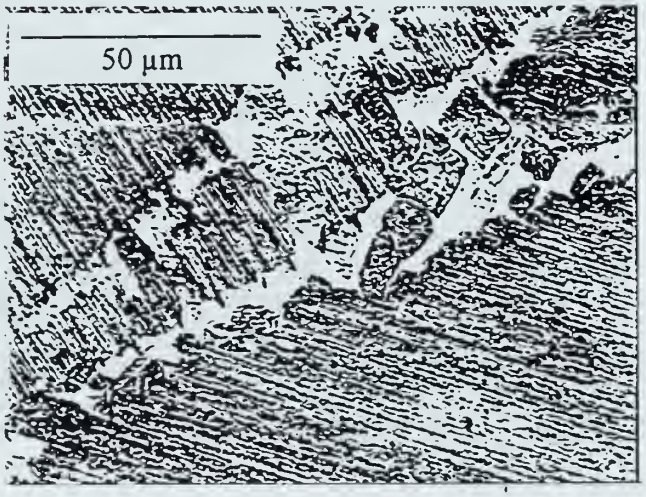

Figure 5.14 Optical micrograph of directionally solidified sample at high magnification

E. SCANNING ELECTRON MICROSCOPY (SEM)

The SEM was used as a tool to analyze the microstructural distribution and chemical composition of the alloys. The specimen surface was scanned visually using secondary electron (SE) imaging. Areas were selected for further analysis based on whether they were typical and representative of the majority of the sample surface or non-typical and worthy of closer inspection to determine the cause for a different appearance.

For selected areas, backscattered electron (BSE) images were recorded using the Oxford Link Isis and Link Tetra software to control the SEM and digitally store the images. A quantitative chemical composition analysis was performed on the x-ray spectra obtained by energy dispersive x-ray spectroscopy (EDX) using the intrinsic germanium x-ray detector. This device detected x-rays and dispersed them into a spectrum according to their energy, which was displayed as a graph of x-ray counts versus x-ray energy. The chemical composition analysis was performed by the SEMQuant software, which performed a line profile analysis, compared the energy peaks detected to reference standards, and performed a ZAF correction for each element. The results were given as weight and atomic percentages of selected element with associated error percentages.

Micrographs of typical microstructure as found in the interior of the chill-cast sample and non-typical microstructure with proportionately large grains as found near the outer edge of the sample are shown in Figures 5.15 and 5.16. Quantitative elemental data for each is indicated beside the micrograph. Figures 5.17 and 5.18 show the EDX spectrum and the SEMQuant results for the typical interior structure of Figure 5.15.

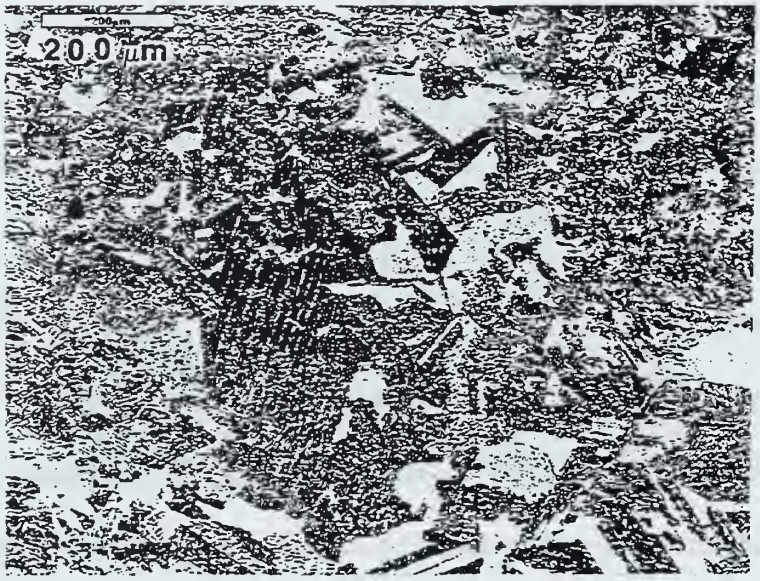

at.%
Ti: 47.02
Al: 43.40
Nb: 9.58

Figure 5.15 BSE micrograph of typical interior microstructure (chill-cast)

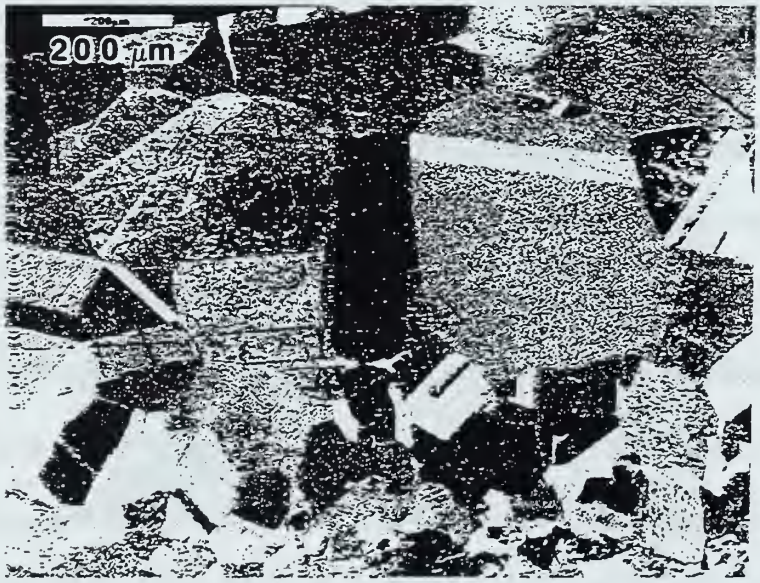

at.%
Ti: 46.94
Al: 43.91
Nb: 9.15

Figure 5.16 BSE micrograph of non-typical edge microstructure (chill-cast)

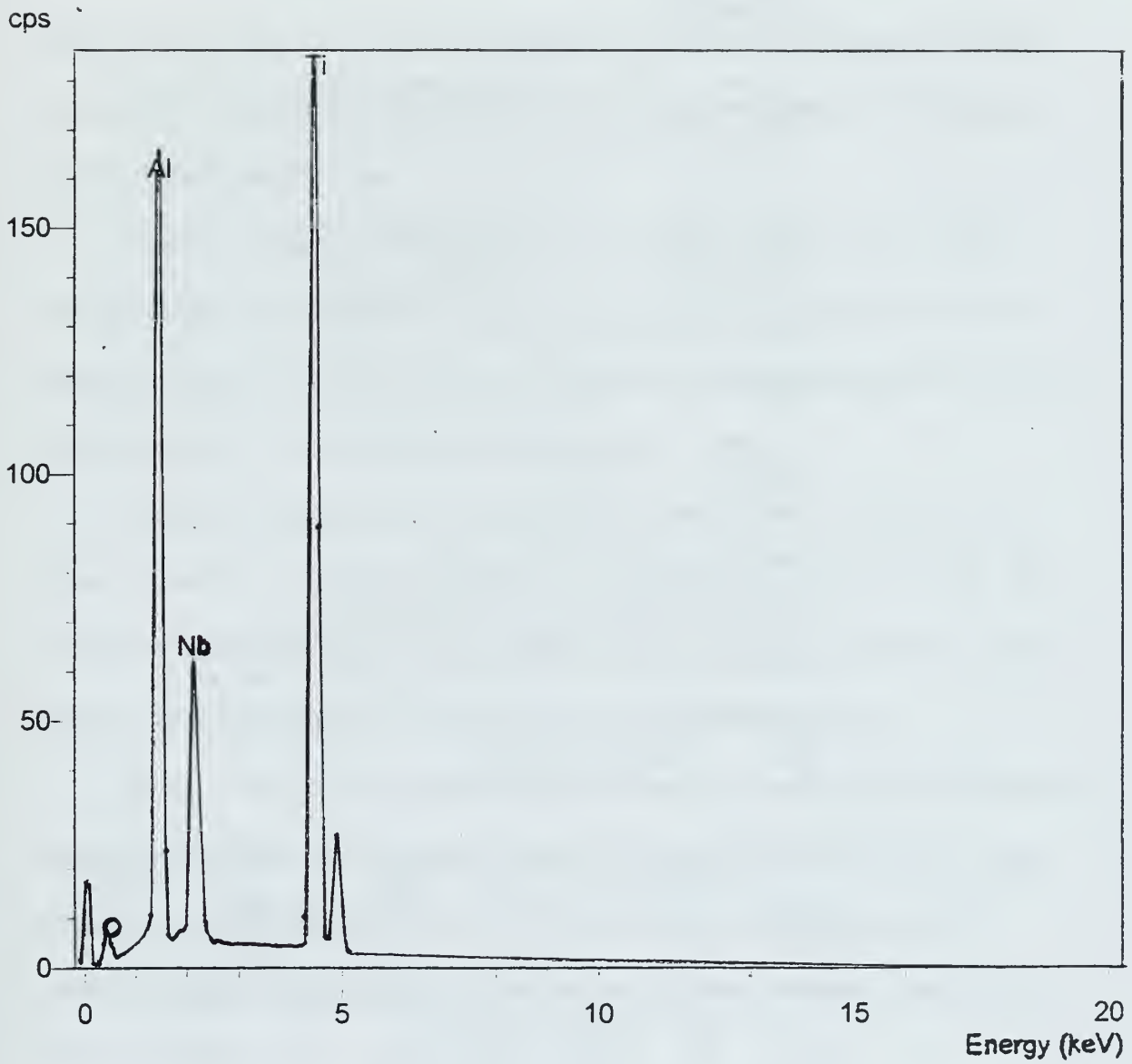

Figure 5.17 EDX spectrum of typical interior microstructure (chill-cast)

```
SEMQuant results. Listed at 9:17:46 PM on 12/22/98
Operator: MENON
Client: Menon
Job: Menon
Spectrum label: tialnb40

Calibration data:     Energy  Resn.   Area
 Strobe:                -7.3 119.91  128152
 Calib. element:      8031.2 176.34  278293
 Gain factor = 49.983
 Livetime     = 174.5 seconds

Sample data:          Energy  Resn.   Area
 Strobe:                -7.2 120.98  117734
 Total spectrum counts = 957182
 Livetime               = 176.1 seconds

System resolution =  126 eV

Geometry (degrees):
 Tilt        =   0.00

ED geometry (degrees):
 Elevation   =  35.00
 Azimuth     =   0.00
 Entry angle =   0.00

Accelerating voltage = 20.00 kV

Quantitative method: ZAF ( 3 iterations).
 Analysed all elements and normalised results.

 3 peaks possibly omitted: 5.94, 11.12, 12.18 keV

Standards :
 Al K      NPS-AlN 7/26/95
 Ti K      NPS-TiC 7/26/95
 Nb L      Nb 07/07/93
```

Elmt	Spect. Type	Fit Index	Apparent Conc.	Stat. Sigma	k ratio	k Ratio Sigma
Al K	ED	530.1	24.058	0.093	0.36547	0.00141
Ti K	ED	404.9	54.717	0.191	0.68438	0.00239
Nb L	ED		17.352	0.162	0.17352	0.00162

Elmt	Spect. Type	Inten. Corrn.	Std Corrn.	Element %	Sigma %	Atomic %
Al K	ED	0.779	1.00	27.15	0.11	43.40
Ti K	ED	0.922	1.00	52.21	0.14	47.02
Nb L	ED	0.740	0.97	20.63	0.16	9.58
Total				100.00		100.00

```
* = <2 Sigma
```

Figure 5.18 SEMQuant data results for typical interior microstructure (chill-cast)

Chemical composition analysis of individual grains and lamellar regions was performed at higher magnifications using the same procedure. The BSE image indicated the relative atomic weights of different structures qualitatively by contrast. A lighter contrast area would have a structure with greater atomic weight than an area with darker contrast. This feature of BSE images allowed differentiation of lamellae within grains at sufficiently high magnifications.

Figures 5.19 through 5.22 illustrate the use of BSE imaging to conduct point chemical composition analysis on selected locations within a structure for both casting structures. Points were evaluated on dark and light regions of lamellar grains as well as in single-phase grains with the results tabulated as shown.

The dark and light phases in these lamellar regions are actually TiAl and Ti_3Al phases, respectively, as confirmed by diffraction and EDX experiments in the TEM. The problem associated with the qualitative EDX in the SEM is that beam spreading in these samples with fine lamellae (<1 μm) leads to incorrect quantitative analysis.

Other methods used for microstructural characterization on the SEM were linescan analysis and elemental x-ray mapping as illustrated in Figures 5.23 through 5.28. These methods provided qualitative comparisons only, but were used to indicate areas of particularly high or low element concentrations for quantitative evaluation using the point analysis method.

Linescan analysis of the chill-cast sample indicated that Al and Nb concentrations varied proportionately in lamellar grains while the Ti concentration remained relatively constant. On the other hand, Al and Nb concentrations were inversely proportional in the

single-phase regions between grains of the directionally solidified sample and the concentrations of all three elements were relatively constant across the lamellar regions of the grains. Elemental x-ray mapping gave the same indications as the linescan data.

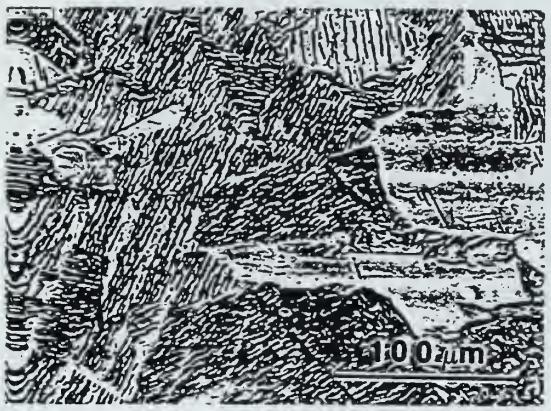

Lamellar (Dk/Lt)		Single Phase
Ti:	56.71 / 46.30	46.93
Al:	34.37 / 44.23	43.51
Nb:	8.92 / 9.47	9.56

Figure 5.19 BSE micrograph of chill-cast interior microstructure (medium mag.)

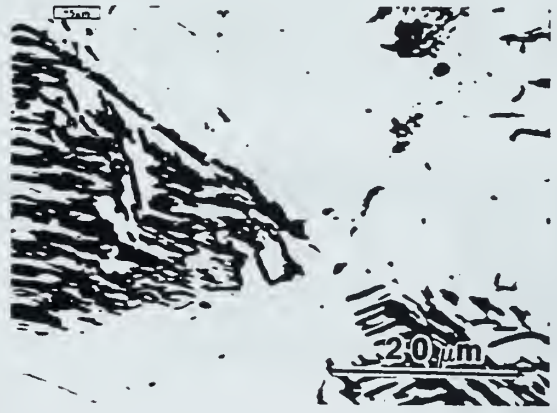

Lamellar (Dk/Lt)		Single Phase
Ti:	50.46 / 45.16	46.77
Al:	40.17 / 45.07	43.29
Nb:	9.38 / 9.78	9.94

Figure 5.20 BSE micrograph of chill-cast interior microstructure (high mag.)

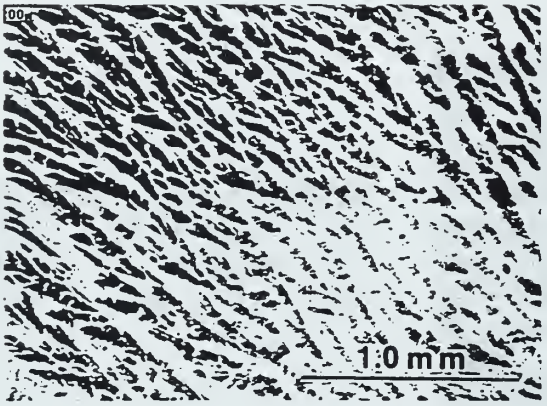

Area Average	
Ti:	45.78
Al:	42.54
Nb:	11.68

Figure 5.21 BSE micrograph of directionally solidified microstructure (low mag.)

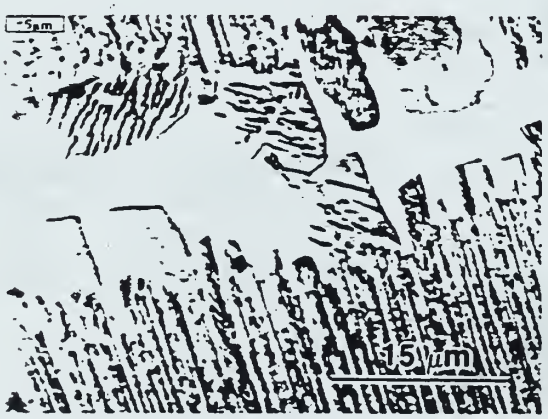

	Lamellar (Dk/Lt)	Single Phase
Ti:	47.23 / 44.79	51.75
Al:	40.58 / 43.51	33.16
Nb:	12.20 / 11.70	15.09

Figure 5.22 BSE micrograph of directionally solidified microstructure (high mag.)

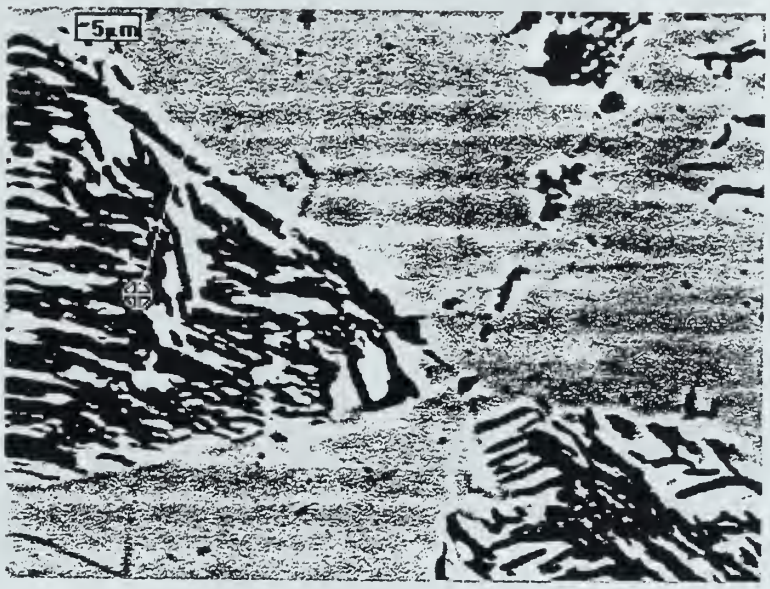

Figure 5.23 BSE micrograph of chill-cast linescan region

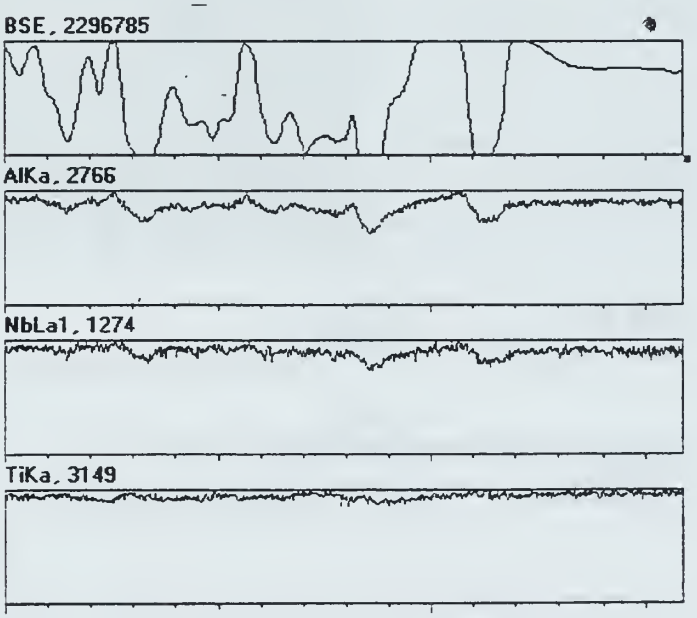

Figure 5.24 Linescan analysis of chill-cast microstructure

Figure 5.25 BSE micrograph of directionally solidified linescan region

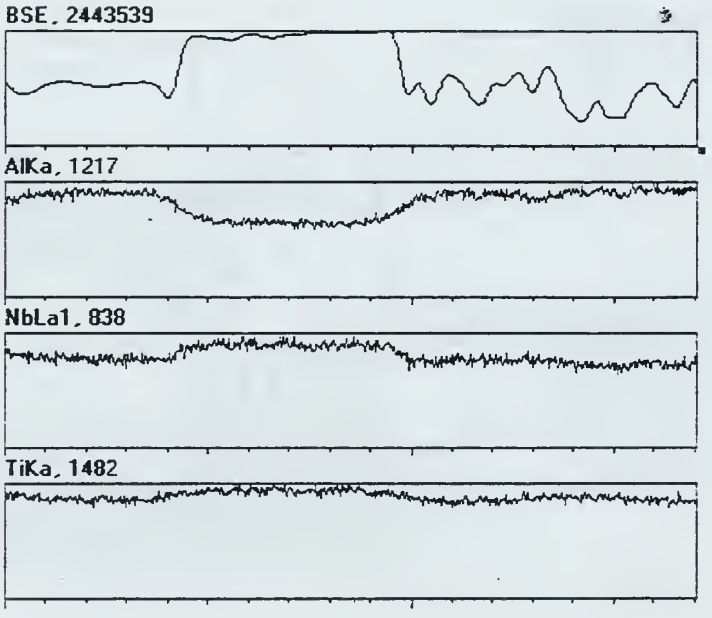

Figure 5.26 Linescan analysis of directionally solidified microstructure

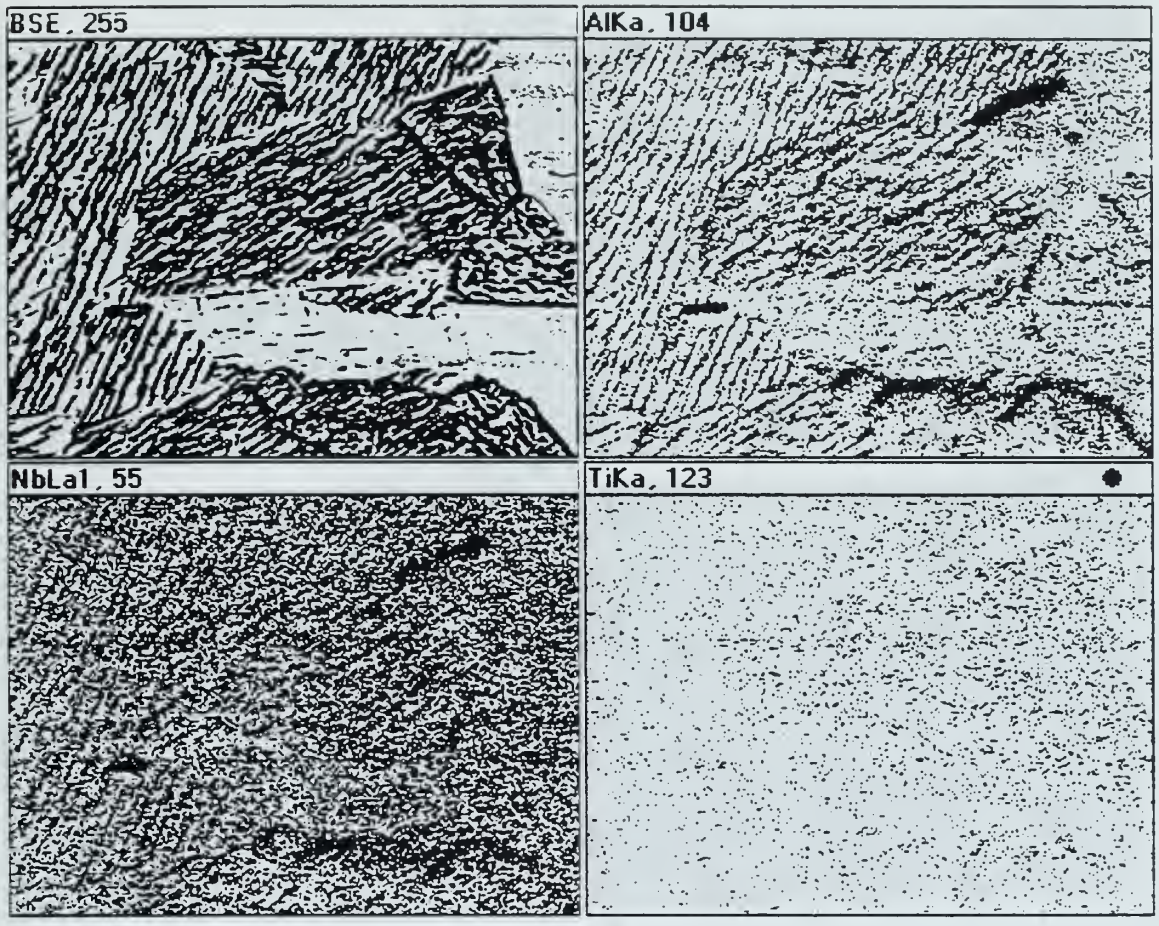

Key:

Darker region: Lower concentration of element

Lighter region: Higher concentration of element

Figure 5.27 Elemental x-ray mapping of chill-cast microstructure

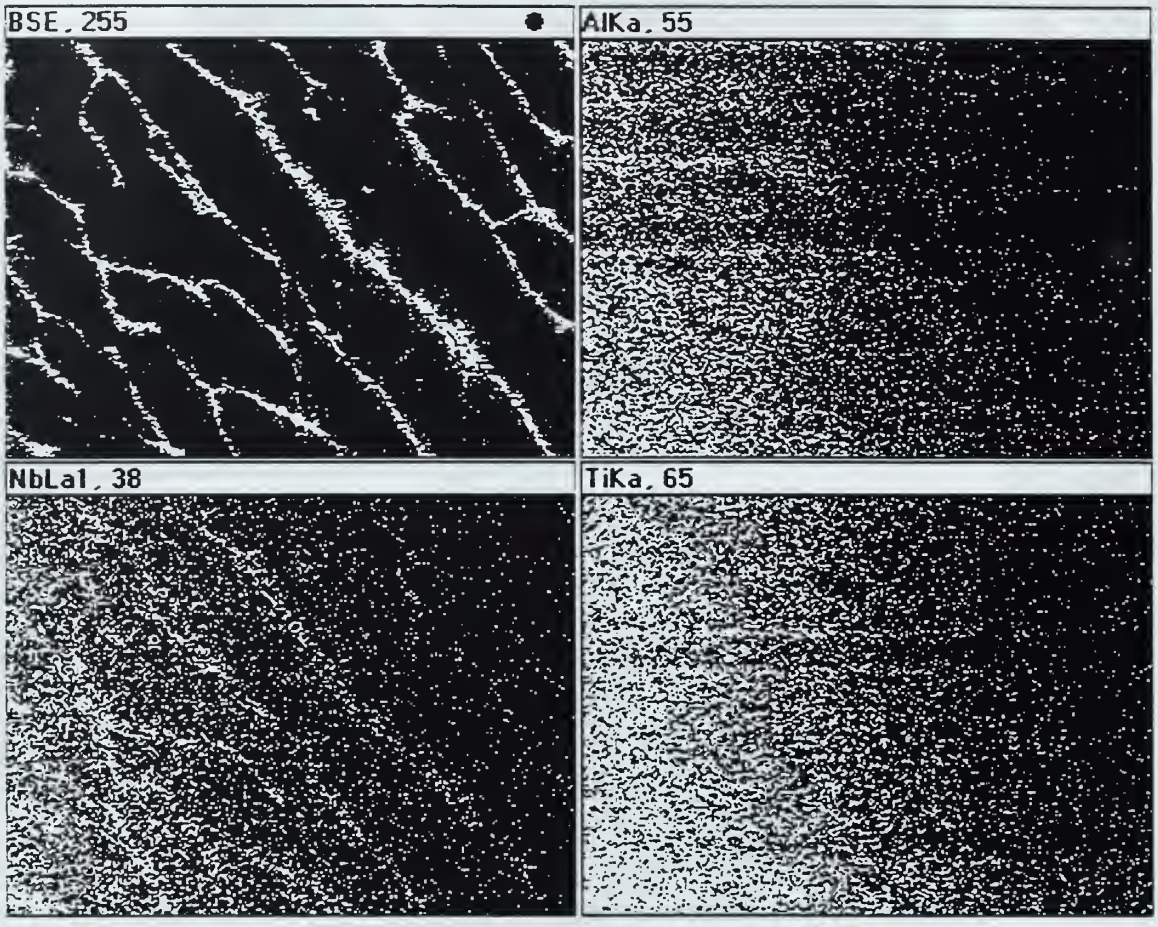

Key:
Darker region: Lower concentration of element
Lighter region: Higher concentration of element

Figure 5.28 Elemental x-ray mapping of directionally solidified microstructure

F. TRANSMISSION ELECTRON MICROSCOPY (TEM)

Analytical procedures on the TEM were similar in some respects to analysis on the SEM. Specimen chemical composition was obtained from selected points in the sample and linescan analysis was performed over features of interest. The advantage of the TEM over the SEM for composition analysis is that it has a much lower error factor due to the narrower probe size, and it has potential for much greater magnification, allowing inspection of smaller features.

The TEM was also used to obtain diffraction patterns in the selected area diffraction (SAD) mode, allowing determination of crystallographic orientation and verification of phases present.

Results from TEM analysis of the chill-cast sample are shown in Figures 5.29 through 5.31. Figure 5.29 shows a linescan analysis of an inter-dendritic region indicating depletion of aluminum in the center region. It appears that during solidification, the Al-rich phase formed first, depleting the surrounding phase in Al. The partitioning of Ti and Nb in this stage appears to be minimal. After the complete solidification of these phases, as the chill-cast samples cooled, further solid state reactions led to more phase transformations. Interestingly enough, the transformations within Al-rich regions of the γ-TiAl phase and separate Ti-rich regions of the same TiAl phase led to formation of $TiAl_3$, and Ti_3Al phases, respectively, as shown in Figures 5.30 and 5.31.

Figure 5.30 shows a linescan across darker needle-like laths of Ti_3Al in a TiAl matrix. The linescan trace clearly indicates high Ti content and Al depletion across the needles, with little variation in Nb content.

Figure 5.31 shows lighter colored needles evaluated to be $TiAl_3$ in a γ-TiAl matrix. The linescan trace indicates titanium depletion in the needle with a corresponding increase of aluminum. Quantitative composition analysis of points in these light colored regions confirmed the presence of the $TiAl_3$ phase with the elemental composition 22.69 at.% Ti, 70.48 at.% Al and 6.82 at.% Nb.

The results of TEM analysis of the directionally solidified sample are shown in Figures 5.32 and 5.33. These samples contained large regions with the lamellar microstructure along with blocky single-phase regions as shown in the micrograph in figure 5.32. EDX data from the large blocky regions showed them to lie in the $TiAl_3$ phase as confirmed by selected area diffraction.

The micrograph shown in Figure 5.33 is a high magnification view of the lamellar region of the directionally solidified sample. The EDX line profile shown in Figure 5.33 shows an inverse variation of Ti with Al in the lamellar regions that was not discernable with SEM analysis, which clearly indicates the alternating TiAl and Ti_3Al phases in the lamellae. Niobium content remains roughly constant in the lamellar region.

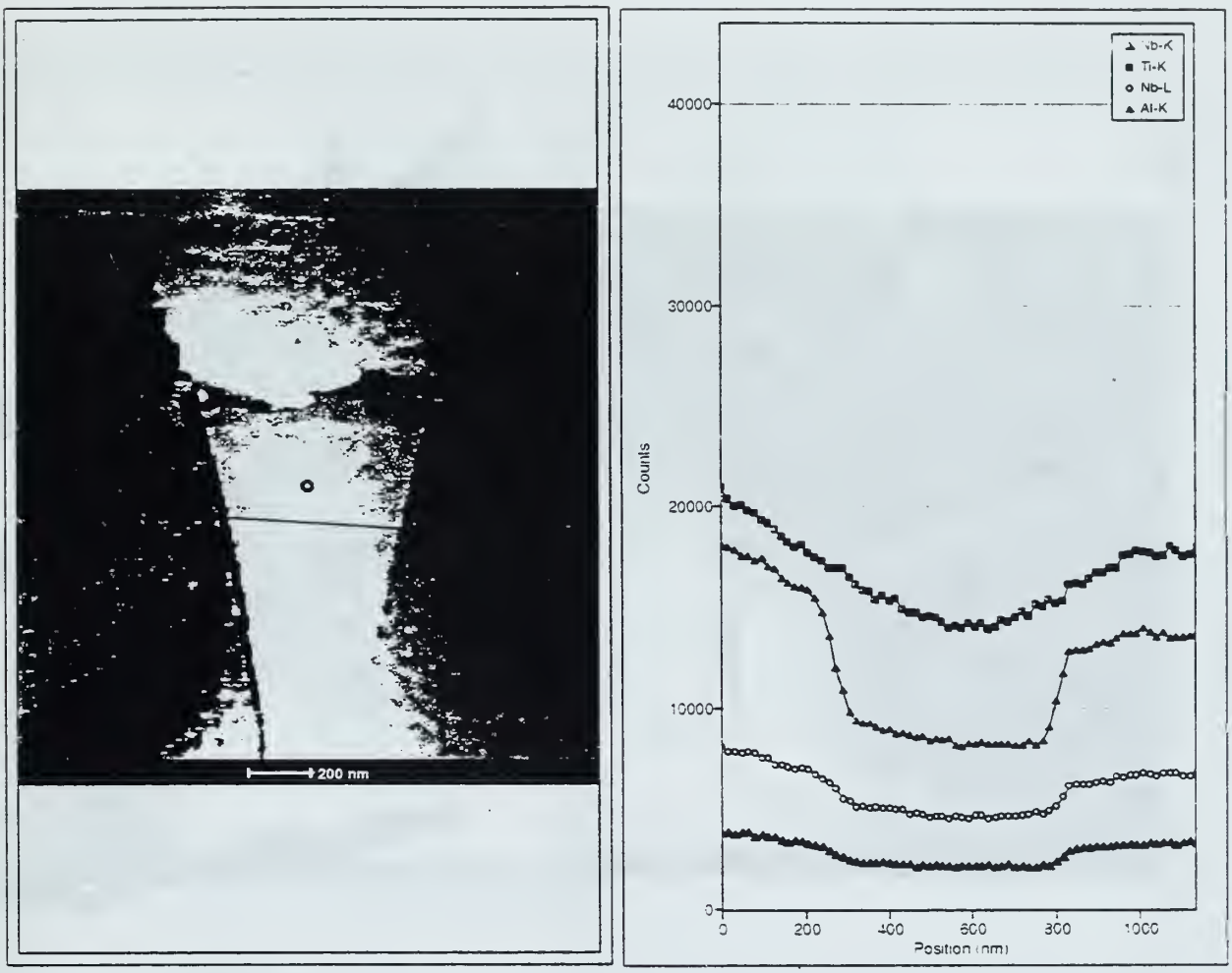

Figure 5.29 Linescan analysis of chill-cast sample in TEM

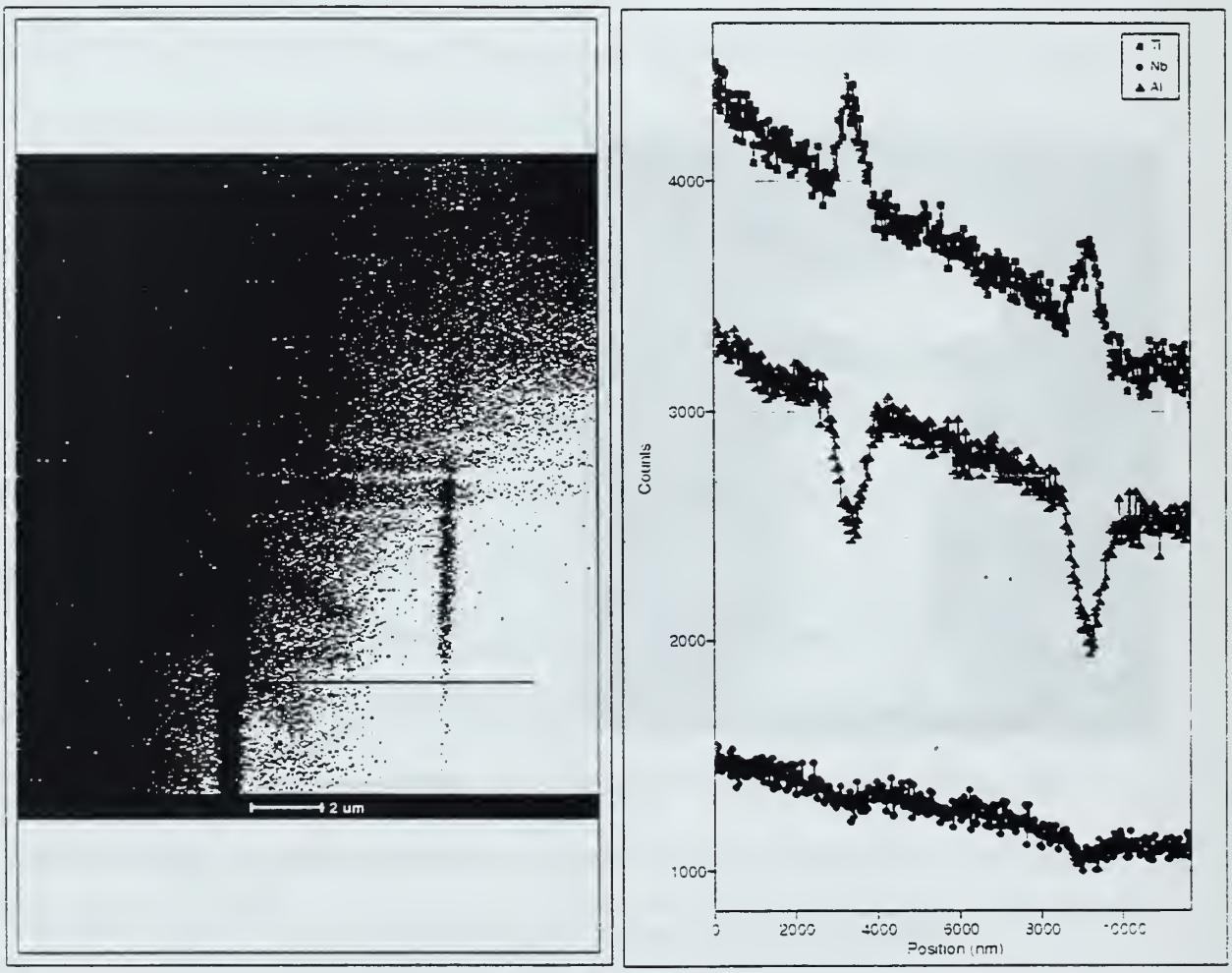

Figure 5.30 TEM linescan analysis of Ti_3Al needles in chill-cast sample

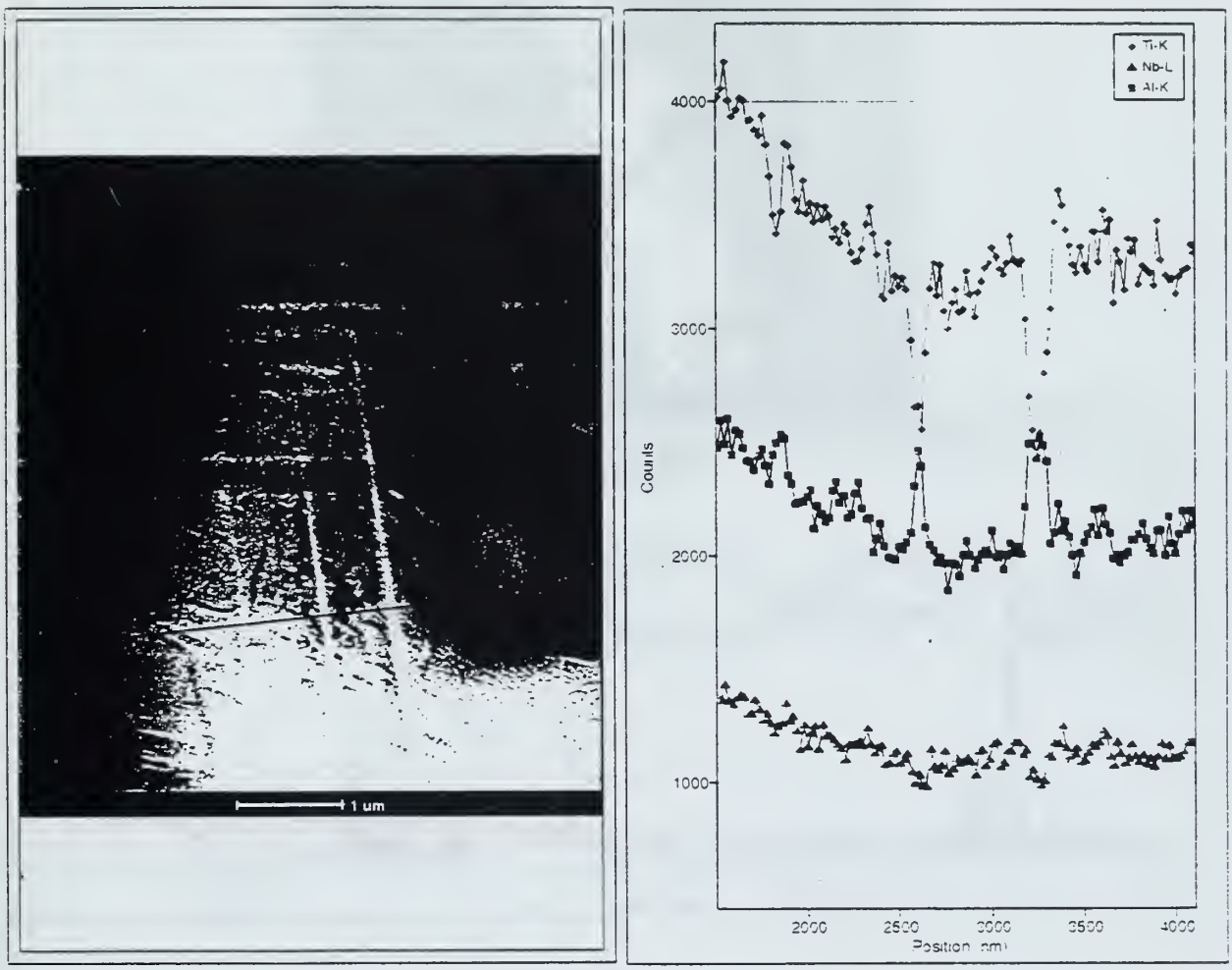

Figure 5.31 TEM linescan analysis of $TiAl_3$ needles in a γ-TiAl matrix

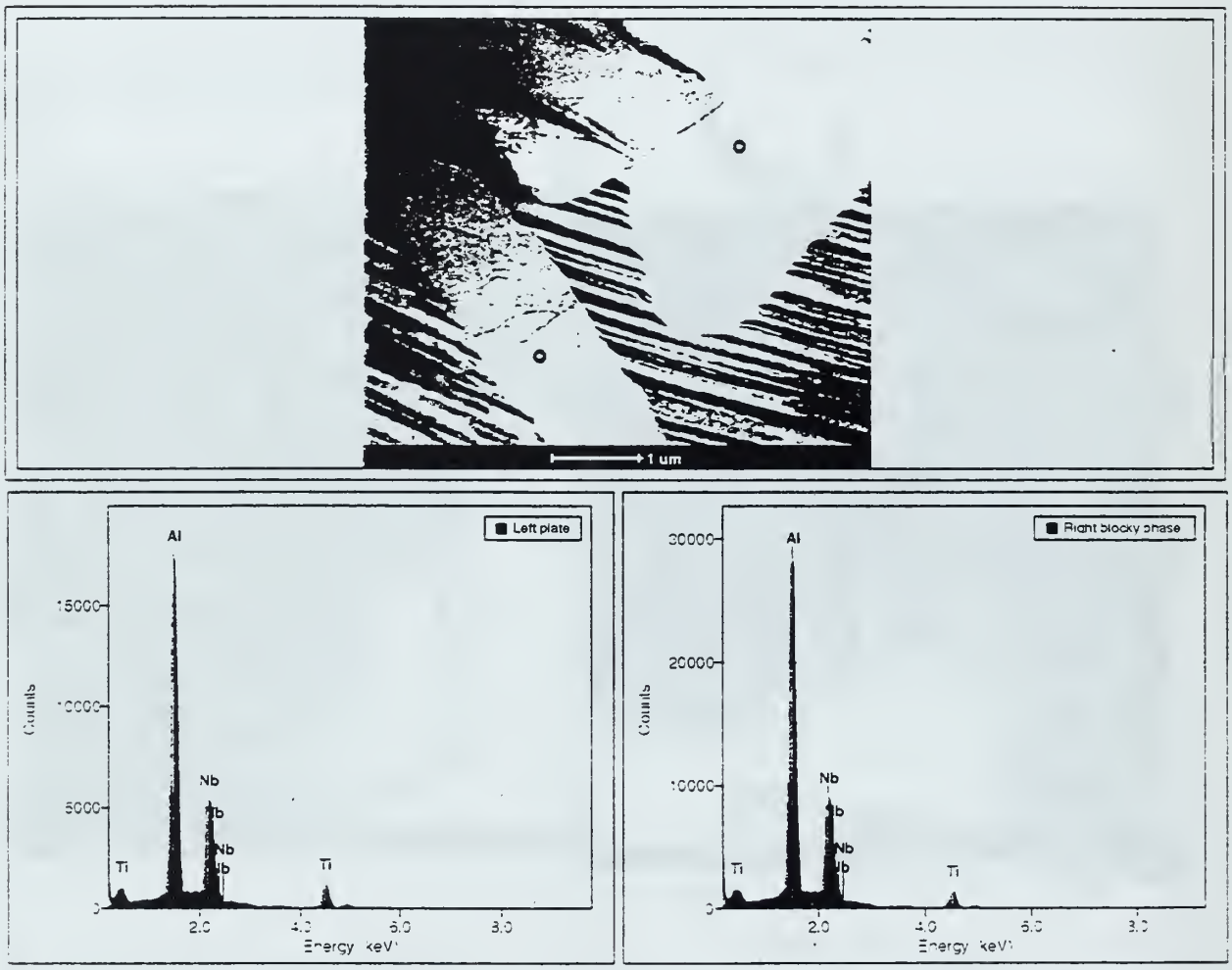

Figure 5.32 TEM EDX spectra of $TiAl_3$ plates in directionally solidified sample

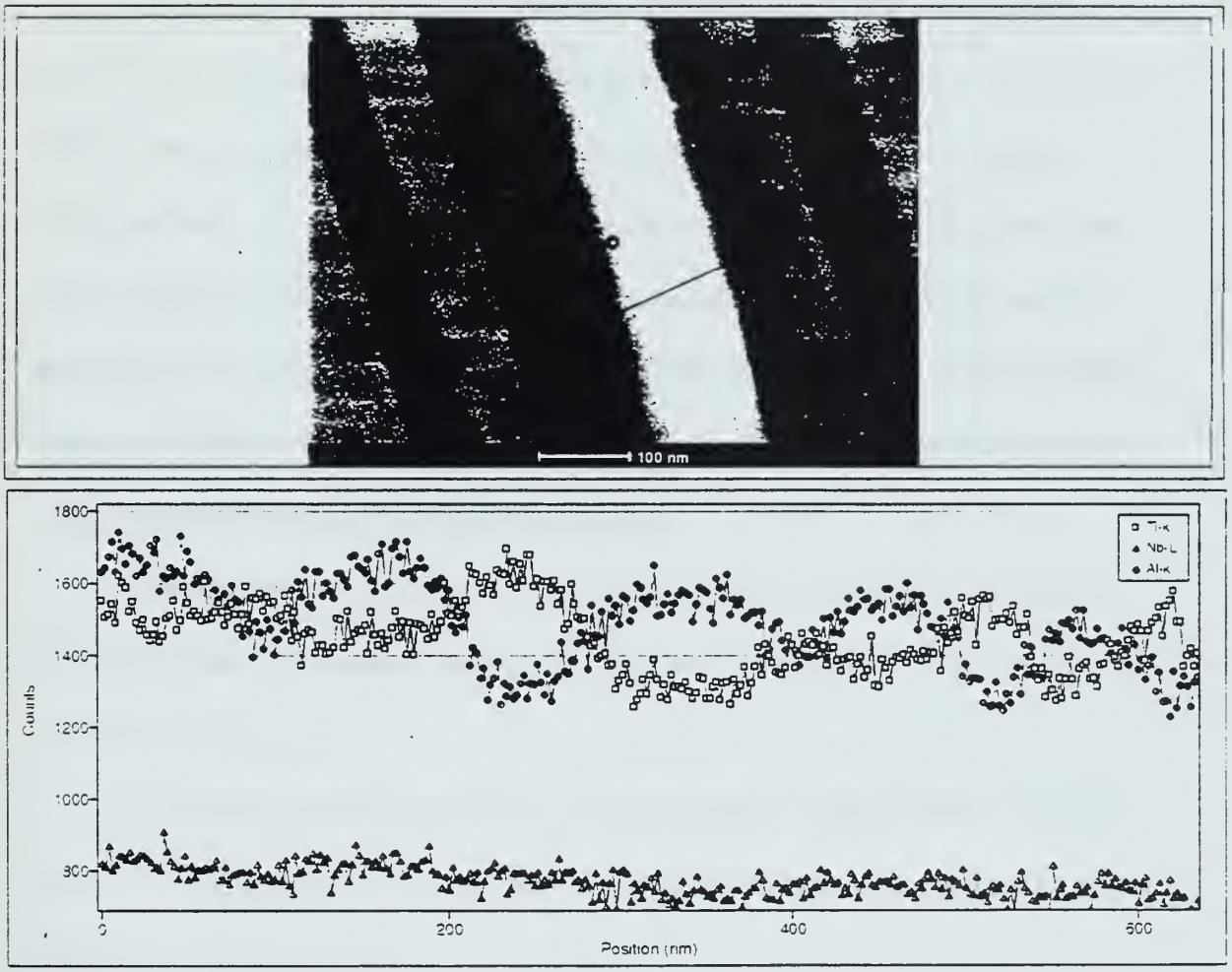

Figure 5.33 TEM linescan analysis of lamellae in directionally solidified sample

VI. SUMMARY

A. CONCLUSIONS

The microstructure of a gamma titanium aluminum alloy with composition Ti-44Al-11Nb (at.%) was studied for two different casting techniques using x-ray diffraction (XRD), scanning electron microscopy (SEM), and transmission electron microscopy (TEM) methods. The as-cast, or chill-cast, sample was studied in the form it developed upon cooling as a button ingot from the original arc-melting without homogenization or any other heat treatments. The directionally solidified sample was initially cast as a button ingot and underwent further processing to achieve a directionally aligned microstructure using the Optical Imaging Floating Zone technique.

Chemical composition of the chill-cast sample varied slightly from the nominal composition due to incomplete melting of niobium, and the resulting inhomogeneity of the remainder of the sample.

Both casting techniques produced the same mixture of phases, which were Al_3Ti, TiAl, and Ti_3Al, with some Nb in solid solution. Within the phases, the microstructural distribution was very different.

The chill-cast sample exhibited a coarse microstructure with large, single-phase γ-TiAl crystals and duplex regions of either ($\gamma + \alpha_2$) or ($\gamma + Al_3Ti$) interspersed throughout the alloy.

The directional solidification technique produced a much more uniform microstructure with fine, equally spaced lamellae oriented parallel to the direction of solidification within each grain. On the macro level, the structure displayed a dendritic appearance with differing orientations of lamellae within the dendrite arms.

Both casting techniques showed enrichment of niobium in interdendritic regions.

B. RECOMMENDATIONS FOR FURTHER STUDY

The majority of the work that has been completed on this study to date has been with x-ray diffraction and scanning electron microscopy. A great deal of work remains to be conducted on the transmission electron microscope, including additional diffraction study and evaluation with parallel energy loss spectroscopy (PEELS), to determine the effect the 11 at.% addition of niobium has on the microstructure of each sample. The presence and segregation, if any, of other elements like oxygen, nitrogen and carbon should be studied by extensive PEELS.

The chill-cast sample did not have the desired elemental composition, so additional samples should be cast, with one or more samples having homogenization and hot isostatic pressing treatments to provide better comparisons for the directionally solidified sample.

Additional research should include different conditions of directional solidification including varying the solidification rate of the samples to determine the optimum velocity of processing, followed by mechanical testing of samples to correlate microstructures with mechanical properties.

LIST OF REFERENCES

1. McAndrew, J.B., and Kessler, H.D., *J. Metals*. (October, 1956) 1348.

2. Kim, Y-W., *Gamma Titanium Aluminides*, eds. Y-W Kim, R. Wagner, and M. Yamaguchi, TMS, PA, (1995), 637.

3. Blackburn, M.J., and Smith, M.P., *U.S. Air Force Report* AFWAL-TR-82-4086 (1982).

4. Huang, S-C, *US Patent*, No. 5,076,858, December 31, 1991.

5. Huang, S-C, and Shih, D.S., *Microstructure/Property Relationships in Titanium Aluminides and Alloys*, ed. Y-W. Kim and R.R. Boyer, TMS, PA, (1990), 105-122.

6. Kim, Y-W., *Acta Metall. Mater.*, 40 (1992), 1121-1134.

7. Shih, D.S., et. al., *Microstructure/Property Relationships in Titanium Aluminides and Alloys*, ed. Y-W. Kim and R.R. Boyer, TMS, PA, (1990), 135-148.

8. Kim, Y-W., *JOM.*, 46(7) (1994), 30-39 and 7.

9. Austin, C.M. and Kelly, T.J., *Gamma Titanium Aluminides*, eds. Y-W Kim, R. Wagner, and M. Yamaguchi, TMS, PA, (1995), 21-32.

10. Nishiyama, Y., Isobe, S., et. al., *High Temperature Aluminides & Intermetallics*, TMS (1990) 557-584.

11. Hartfield-Wunsch, S.E., Sperling, A.A., Morrison, R. S., Dowling, Jr., W.E., and Allison, J.E., *Gamma Titanium Aluminides*, eds. Y-W Kim, R. Wagner, and M. Yamaguchi, TMS, PA, (1995), 41-52.

12. Murray, J.L., *Binary Alloy Phase Diagrams*, Vol. 1, eds. T.B. Massalski, H. Okamoto, P.R. Subramanian, L. Kacprzak, ASM International, (1990), 226.

13. Kim, Y-W., Dimiduk, D.M., *JOM.*, 43(8) (1991), 40-47.

14. Kim, Y-W., *High-Temperature Ordered Intermetallic Alloys IV*, ed. J.O. Stiegler, L.A. Johnson, and D.P. Pope, Pittsburgh, PA: MRS, (1991), 777-794.

15. Veeraraghavan, D., Pilchowski, U., Natarajan, B. and Vasudevan, V.K., *Acta Materiala*, 46(2) (1998), 405-421.

16. Perepezko, J.H., Chang, Y.A., Setzman, L.E., Lin, L.C., Bonda, N.R., Jewett, T.J. and Mishurda, J.C., *High Temperature Aluminides and Intermetallics*, TMS (1990), 19.

17. Kim, Y-W., Dimiduk, D.M., *Proc. JIMIS-7 on High Temp. Deformation and Fracture*, (JIM, Nagoya, Japan, 1993), 373-382.

18. Chan, K.S., and Kim, Y-W, *Metall. Trans. A*, 23A (1992), 1663-1677.

19. Chan, K.S., and Kim, Y-W, *Metall. Trans. A*, 24A (1993), 113-125.

20. Kim, Y-W, *Materials Sci. & Eng.*, A192/193 (1995), 519-533.

21. Kim, Y-W, *Intermetallic Compounds*, eds. M. Yamaguchi and H. Fukutomi, 3rd Japan Int'l SAMPE Symp., (Chiba, Japan, December 7-9 1993), 1310-1317.

22. Tsuyama, S., Mitao, S. Minakawa, K., *Materials Sci. & Eng.*, A153 (1992), 451-456.

23. Huang, J.S., and Kim, Y-W, *Scripta Metall.*, 25 (1991), 1901-1906.

24. Kumpfert, J., Kim, Y-W, and Dimiduk, D.M., *Materials Sci. & Eng.*, A192/193 (1995), 465-473.

25. Vaidya, W.V., Schwalbe, K-H., and Wagner, R., *Gamma Titanium Aluminides*, eds. Y-W Kim, R. Wagner, and M. Yamaguchi, TMS, PA, (1995), 867-874.

26. Bowen, P., Rogers, N.J., James, A.W., *Gamma Titanium Aluminides*, eds. Y-W Kim, R. Wagner, and M. Yamaguchi, TMS, PA, (1995), 849-866.

27. Khataee, A., Flower, H.M., West, D.R.F., *J. Materials Engineering.*, 10(1) (1988), 37-44.

28. Khataee, A., Flower, H.M., West, D.R.F., *Platinum Metals Rev.*, 33(3) (1989), 106-113.

29. Hall, E.L., and Huang, S.C., *High-Temperature Ordered Intermetallic Alloys III*, ed. C.T. Liu et. al. (Pittsburgh, PA: MRS 1989), 693-698.

30. Maykuth, D.J., Battelle, DMIC Report 136B (May 29,1961).

31. Martin, P.L., Lipsitt, H.A., Nuhfer, N.T., Williams, J.C., "The Effects of Alloying on the Microstructure of Ti_3Al and TiAl", *Ti'80, Sci. and Tech.* (1980), 1245-1254.

32. Singh, A.K., and Banerjee, D., *Metall. and Mat. Trans. A*, 28A (1997), 1735-1743.

33. Singh, A.K., and Banerjee, D., *Metall. and Mat. Trans. A*, 28A (1997), 1745-1753.

34. Kawabata, T., Fukai, H., Izumi, O., *Acta Mater.*, 46(6) (1998), 2185-2194.

35. Cheng, T.T. and Loretto, M.H., *Acta Mater.*, 46(13) (1998), 4801-4819.

36. Yu, T.H. and Koo, C. H., *Scripta Mater.*, 39(7) (1998), 915-922.

37. Wang, J.G., Zhang, L.C., Chen, G.L. and Ye, H.Q., *Materials Sci. & Eng.*, A252 (1998), 222-231.

38. Paul, J.D.H., Appel, F., Wagner, R., *Acta Mater.*, 46(4) (1998), 1075-1085.

39. Konitzer, D.G., Jones, I.P. and Fraser, H.L., *Scripta Metall.*, 20(2) (1986), 265-268.

40. Mohandas, E. and Beaven, P.A., *Scripta Metall. et Mater.*, 25(9) (1991), 2023-2027.

41. Rossouw, C.J., Forwood, C.T., Gibson, M.A. and Miller, P.R., *Phil. Mag. A*, 74 (1996), 57-77.

42. Yamaguchi, M., Inui, H., Yokoshima, S. Kishida, K., Johnson, D.R., *Materials Sci. & Eng.*, A213 (1996), 25-31.

43. Kim, M.C., Oh, M.H., Lee, J.H., Inui, H., Yamaguchi, M., Wee, D.M., *Materials Sci. & Eng.*, A239-240 (1997), 570-576.

44. Johnson, D.R., Inui, H., Yamaguchi, M., *Acta Mater.*, 44(6) (1996), 2523-2535.

45. Johnson, D.R., Masuda, Y., Inui, H., Yamaguchi, M., *Acta Mater.*, 45(6) (1997), 2523-2533.

46. Johnson, D.R., Masuda, Y., Inui, H., Yamaguchi, M., *Materials Sci. & Eng.*, A239-240 (1997), 577-583.

47. Menon, E.S.K. and Fox, A.G., *Phil. Mag. A*, 77(3) (1998), 577-592.

48. Mahapatra, R., "Deformation Mechanisms of Single-Phase TiAl Single Crystals", PhD Dissertation, Lehigh University, PA, 1996.

49. Williams, B.D., and Carter, C.B., *Transmission Electron Microscopy*, Plenum Press, 1996.

INITIAL DISTRIBUTION LIST

1. Defense Technical Information Center 2
   8725 John J. Kingman Road, STE 0944
   Ft. Belvoir, Virginia 22060-6218

2. Dudley Knox Library 2
   Naval Postgraduate School
   411 Dyer Road
   Monterey, California 93943-5100

3. Naval/Mechanical Engineering, Code 34 1
   Naval Postgraduate School
   700 Dyer Road, Bldg. 245
   Monterey, California 93943-5100

4. Department Chairman, Code ME/Mc 1
   Department of Mechanical Engineering, NPS
   700 Dyer Road, Bldg. 245
   Monterey, California 93943-5100

5. Dr. Alan G. Fox, Code ME/Fx 2
   Department of Mechanical Engineering, NPS
   700 Dyer Road, Bldg. 245
   Monterey, California 93943-5100

6. Dr. Sarath Menon, Code ME/Ms 1
   Department of Mechanical Engineering, NPS
   700 Dyer Road, Bldg. 245
   Monterey, California 93943-5100

7. Dr. Rabin Mahapatra 1
   Mail Stop 08, Materials Bldg. (2188)
   Naval Air Warfare Center
   22251 Millstone Road
   Patuxent River, Maryland 20670

8. LT Tim Halladay 2
   225 Cactus Road
   Belgrade, Montana 59714

12 483NPG 3144
TH
10/99 22527-200 NRLF

DUDLEY KNOX LIBRARY
3 2768 00366277 6